mathematics

MDPI

Article

Complete Balancing of the Six-Bar Mechanism Using Fully Cartesian Coordinates and Multiobjective Differential Evolution Optimization

María T. Orvañanos-Guerrero [1], Mario Acevedo [2], Claudia N. Sánchez [1], Daniel U. Campos-Delgado [3], Amir Aminzadeh Ghavifekr [4], Paolo Visconti [1,5] and Ramiro Velázquez [1,*]

1 Facultad de Ingeniería, Universidad Panamericana, Aguascalientes 20290, Mexico; torvananos@up.edu.mx (M.T.O.-G.); cnsanchez@up.edu.mx (C.N.S.); paolo.visconti@unisalento.it (P.V.)
2 Facultad de Ingeniería, Universidad Panamericana, Zapopan 45010, Mexico; macevedo@up.edu.mx
3 Facultad de Ciencias, Instituto de Investigación en Comunicación Óptica, Universidad Autónoma de San Luis Potosí, San Luis Potosí 78295, Mexico; ducd@fciencias.uaslp.mx
4 Faculty of Electrical and Computer Engineering, University of Tabriz, Tabriz 5166616471, Iran; aa.ghavifekr@tabrizu.ac.ir
5 Department of Innovation Engineering, University of Salento, 73100 Lecce, Italy
* Correspondence: rvelazquez@up.edu.mx; Tel.: +52-449-910-6200

Abstract: The high-speed operation of unbalanced machines may cause vibrations that lead to noise, wear, and fatigue that will eventually limit their efficiency and operating life. To restrain such vibrations, a complete balancing must be performed. This paper presents the complete balancing optimization of a six-bar mechanism with the use of counterweights. A novel method based on fully Cartesian coordinates (FCC) is proposed to represent such a balanced mechanism. A multiobjective optimization problem was solved using the Differential Evolution (DE) algorithm to minimize the shaking force (ShF) and the shaking moment (ShM) and thus balance the system. The Pareto front is used to determine the best solutions according to three optimization criteria: only the ShF, only the ShM, and both the ShF and ShM. The dimensions of the counterweights are further fine-tuned with an analysis of their partial derivatives, volumes, and area–thickness relations. Numerical results show that the ShF and ShM can be reduced by 76.82% and 77.21%, respectively, when importance is given to either of them and by 45.69% and 46.81%, respectively, when equal importance is given to both. A comparison of these results with others previously reported in the literature shows that the use of FCC in conjunction with DE is a suitable methodology for the complete balancing of mechanisms.

Keywords: six-bar mechanism; dynamic balancing; fully Cartesian coordinates; multiobjective optimization; differential evolution; Pareto front

MSC: 91B03; 70B15

Citation: Orvañanos-Guerrero, M.T.; Acevedo, M.; Sánchez, C.N.; Campos-Delgado, D.U.; Ghavifekr, A.A.; Visconti, P.; Velázquez, R. Complete Balancing of the Six-Bar Mechanism Using Fully Cartesian Coordinates and Multiobjective Differential Evolution Optimization. *Mathematics* **2022**, *10*, 1830. https://doi.org/10.3390/math10111830

Academic Editors: Higinio Rubio Alonso, Alejandro Bustos Caballero, Jesus Meneses Alonso and Enrique Soriano-Heras

Received: 23 April 2022
Accepted: 21 May 2022
Published: 26 May 2022

1. Introduction

The high-speed motion of the links of a mechanism generates dynamic reactions that are transmitted as vibrations to the fixed frame producing undesirable effects such as noise, wear, fatigue, and energy losses that will eventually limit the mechanism's performance and operating life. In addition to these technical problems, vibrations may induce a constant machine maintenance involving wastes that have an environmental impact and noise pollution that can lead to health problems [1].

The dynamic reactions under discussion are produced by both external and inertial forces. The former are naturally forces generated outside the mechanism such as those induced by an actuator. The latter are due to the large accelerations of the links. Some representative methods for calculating dynamic reactions in mechanisms are those of Uicker [2] and Waldron [3].

The force and the moment that occur at the mechanism's fixed frame are typically known as shaking force (ShF) and shaking moment (ShM), respectively. Thus, a traditional but still open challenge in machine theory is how to effectively remove or minimize the dynamic reactions, i.e., the ShF and ShM, derived from the mechanism's motion. This process is known as complete (or dynamic) balancing.

The dynamic balancing of mechanisms has been widely studied in mechanical engineering. Some recent historical reviews addressing the topic can be found in [1,4–6].

Among the first publications, we can find the work of Fischer introducing in 1902 a method called principal vectors [7]. This method allows for the balancing of the ShF by analyzing each of the links of the mechanism and determining the points, called principal points, in which the static balancing can be reached. The work of Fischer provided the basis for the methods studying the motion of the centers of mass (CoM) of the links in a mechanism. The method of principal vectors was subsequently used by Goryachkin [8], Yudin [9], and Kreutzinger [10].

Another early method proposed for the dynamic balancing of mechanisms was the static substitution of masses. Its aim is to statically replace the mass of the coupler by concentrated masses, thus transforming the problem of mechanism balancing into a simpler problem of balancing the rotating links. The works of Maxwell [11], Smith [12], and Talbourdet [13] are based on this method.

The 1920s were marked by a special interest in the balancing of engines [14,15] and machines related to agriculture [16]. The Lanchester balancer stands out among these works. It is still being used for balancing four-stroke engines.

During the 1940s, some methods based on function approximation were proposed to achieve partial equilibrium. The work of Gheronimus [17] is a representative example. In this work, the balancing conditions were formulated by minimizing the root mean square (RMS) or the maximum values of the ShM. The duplicate mechanism method [18] was also proposed in this decade. It achieves a complete balancing with the addition of axial and mirror symmetric mechanism duplicates.

The balancing methods based on harmonic analysis appeared in the 1960s with the use of the crank-slider mechanism in internal combustion engines [19,20]. Such methods reduce the ShM by balancing certain harmonics of both the ShF and ShM. To carry out this process, the unbalanced forces and moments are divided into Fourier series and then analyzed in parts.

In 1969, Berkof and Lowen [21] proposed a new solution for dynamic balancing using a method called linearly independent vectors. This method consists of formulating an equation considering a vector representation describing the position of the total CoM of the mechanism in conjunction with the equation representing the closed kinematic chain. A system of equations containing linearly independent vectors is then obtained allowing to find the balancing conditions of the mechanism by reducing to zero the time-dependent coefficients. This method was subsequently explored in [22,23].

In the 1970s, the dynamic balancing theory achieved significant advances. Berkof [24] formulated the first method for complete balancing using counterweights and counter-inertias to eliminate the undesired forces and moments of the moving links, respectively. It then became clear that a complete balancing of mechanisms is feasible at the expense of considering complex design modifications and an inevitable increase of the total mass and volume of the mechanism.

Methods proposing a partial balancing were then proposed searching to keep the added mass reasonably small. In [25], Wiederrich and Roth formulated simple general conditions for determining the inertia properties of a four-bar mechanism and achieved its partial balancing. Dresig examined the partial balancing conditions for several 2D mechanims with six and eight-bar linkages [26].

Later approaches involved the use of planetary [27] and auto-balanced systems [28]. More recent ones propose the use of the instantaneous dynamic balancing conditions [29], the trajectory planning of the CoM of the mechanism [30], and the reformulation of the

balancing conditions following a Taylor-based approach [29]. Finally, the most recent and novel balancing method encompasses the flexibility of the links of the mechanism [31].

We focus our attention on Berkof's counterweight approach. After the partial balancing methods, optimization techniques were then explored searching a tradeoff between the added mass and the reduction of the ShF and ShM.

In 1998, Segla presented the static balancing optimization of a robotic mechanism [32]. The balancing conditions were first obtained and then, a basic genetic algorithm programmed in Fortran was used for the optimization.

Currently, the most popular optimization techniques for mechanical problems are based on metaheuristic methods: evolutionary [33], differential evolution [34], genetic [35], and Firefly [36] algorithms. These proposals were designed to find heuristics (i.e., partial solutions) that may provide sufficiently good tradeoffs for the dynamic balancing problem.

To our knowledge, all previous works addressing optimization techniques for the dynamic balancing of mechanisms make use of Cartesian coordinates (CC) to obtain the expressions of the dynamic reactions. A major drawback of CC is that they involve trigonometric functions that derive into complex mathematical expressions that are computationally burdensome.

Our research approach differs from the existing literature in that it presents an alternative to CC: fully Cartesian coordinates (FCC), which are also called natural coordinates [37]. By using FCC, the dynamic reactions at the fixed frame can be formulated by means of equations of less complexity (no angular variables). Then, the resulting ShF and ShM expressions are used to optimize the dynamic balancing of mechanisms through the use of counterweights.

Our previous work [38,39] successfully reported the dynamic balancing of a four-bar mechanism and its optimization with Projected Gradient Descent. In this paper, we address the dynamic balancing of a more complex system, a six-bar mechanism, and explore the differential evolution (DE) algorithm as our optimization method.

Parallel mechanisms are increasingly being used in robotic applications [40,41]. The six-bar mechanism is a typical parallel manipulator. This single degree-of-freedom planar linkage is typically used as a variable-speed transmission mechanism where the input crank rotates at constant speed and the output link works as an overrunning clutch mounted on the output shaft [42].

The rest of the paper is organized as follows: In Section 2, the FCC-based mass-matrix definition for the six-bar mechanism with counterweights is introduced together with the expressions of the ShF and ShM. In Section 3, the details of the multiobjective DE optimization are presented. In Section 4, a numerical example is presented to illustrate the proposed approach. In Section 5, results are discussed and compared to others previously reported in the literature. Finally, Section 6 concludes, summarizing the main contributions and giving the future work perspectives of this research.

2. Mechanical Analysis

2.1. FCC-Based Definition of the Mass Matrix of an Element Defined by Three Basic Points

This section details the method used to obtain the mass matrix $\mathbf{M_{3P}}$ of elements defined by three basic points using FCC and the concept of virtual work.

Consider an element defined by three basic points i, j, and k, as shown in Figure 1. The element is located in a global coordinate system (x, y) and in a local coordinate system $(\bar{x}, \bar{y})$ with its origin at point i and the $\bar{x}$ axis directed toward point j.

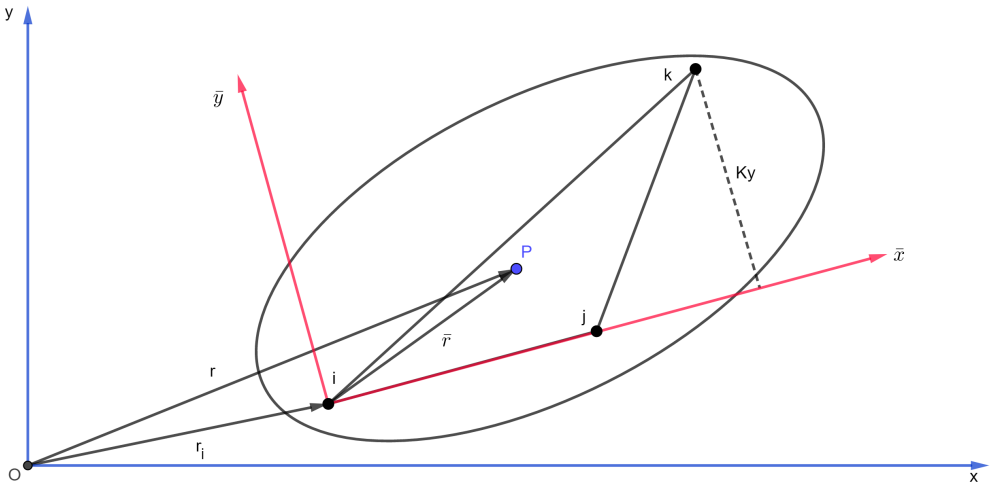

Figure 1. A 2D element with three basic points (i, j, and k).

The location of any point P in this element is defined by a vector $\mathbf{r}$ in the global reference system and a vector $\bar{r}$ in the local coordinate system. In this way, $\mathbf{r}$ can be expressed, according to Equation (1).

$$\mathbf{r} = \mathbf{r_i} + \mathbf{A}\bar{\mathbf{r}} \tag{1}$$

where $\mathbf{A}$ is the rotation matrix. Being the element rigid, the local position of vector $\bar{\mathbf{r}}$ remains constant regardless of the element's motion. Thus, the position of point P can be defined according to Equation (2).

$$\mathbf{r} = \mathbf{r_i} + \mathbf{A}\bar{\mathbf{r}} = \mathbf{r_i} + c_1(\mathbf{r_j} - \mathbf{ri}) + +c_2(\mathbf{r_k} - \mathbf{r_i}) \tag{2}$$

where c_1 and c_2 are the components of vector $\bar{\mathbf{r}}$ in the local coordinate system. The components of vector $\mathbf{r}$ can be expressed in matrix form as shown in Equation (3).

$$\mathbf{r} = \begin{Bmatrix} x \\ y \end{Bmatrix} = \begin{bmatrix} 1-c_1-c_2 & 0 & c_1 & 0 & c_2 & 0 \\ 0 & 1-c_1-c_2 & 0 & c_1 & 0 & c_2 \end{bmatrix} \begin{Bmatrix} x_i \\ y_i \\ x_j \\ y_j \\ x_k \\ y_k \end{Bmatrix} = \mathbf{Cq} \tag{3}$$

where $\mathbf{q}^{\mathbf{T}} = \{x_i \quad y_i \quad x_j \quad y_j \quad x_k \quad y_k\}$ is the vector that contains the FCC of the element. Note that matrix $\mathbf{C}$ is constant for a given point P and does not change with the system's motion, thus fulfilling Equations (4) and (5).

$$\dot{\mathbf{r}} = \mathbf{C}\dot{\mathbf{q}} \tag{4}$$

$$\ddot{\mathbf{r}} = \mathbf{C}\ddot{\mathbf{q}} \tag{5}$$

Coefficients c_1 and c_2 in matrix $\mathbf{C}$ can be expressed in terms of the coordinates of points i, j, and k in the local reference frame according to Equation (6).

$$\bar{\mathbf{r}} = c_1(\mathbf{r_j} - \mathbf{r_i}) + c_2(\mathbf{r_k} - \mathbf{r_i}) \tag{6}$$

Since $\bar{\mathbf{r_i}} = 0$ is located at the local reference origin, Equation (6) can be rewritten as shown in Equation (7).

$$\bar{\mathbf{r}} = [\ \bar{\mathbf{r_j}} \mid \bar{\mathbf{r_k}}\ ] \begin{Bmatrix} c_1 \\ c_2 \end{Bmatrix} = \bar{\mathbf{X}}\mathbf{c} \tag{7}$$

Vector $\mathbf{c}$ contains the coefficients c_1 and c_2, and matrix $\bar{\mathbf{X}}$ has the components of vectors $\bar{\mathbf{r}}_\mathbf{j}$ and $\bar{\mathbf{r}}_\mathbf{k}$ in its columns (Equation (8)).

$$\bar{\mathbf{X}} = [\ \bar{\mathbf{r}}_\mathbf{j} \mid \bar{\mathbf{r}}_\mathbf{k}\ ] = \begin{bmatrix} x_j & x_k \\ y_j & y_k \end{bmatrix} = \begin{bmatrix} l_{ij} & K_x \\ 0 & K_y \end{bmatrix} \tag{8}$$

Now, it is possible to define the virtual work W^* generated by the inertial forces (Equation (9)).

$$W^* = -\rho \int_\Omega \dot{\mathbf{r}}^{*T} \ddot{\mathbf{r}} d\Omega \tag{9}$$

where ρ is the density of the element's material. Substituting Equations (4) and (5) into Equation (9) yields to the definition of virtual work (Equation (10)):

$$W^* = -\rho \int_\Omega \dot{\mathbf{q}}^{*T} \mathbf{C}^\mathbf{T} \mathbf{C} \ddot{\mathbf{q}} d\Omega \tag{10}$$

Since vectors $\dot{\mathbf{q}}^{*\mathbf{T}}$ and $\ddot{\mathbf{q}}$ are independent of Ω, they can be taken out of the integral as expressed by Equation (11).

$$W^* = -\dot{\mathbf{q}}^{*T} \left(\rho \int_\Omega \mathbf{C}^\mathbf{T} \mathbf{C} d\Omega \right) \ddot{\mathbf{q}} \tag{11}$$

On the other hand, taking into account the definition of virtual work proposed in [43] (Equation (12)) and comparing it to Equation (11), the mass matrix $\mathbf{M_{3P}}$ can be expressed by Equation (13).

$$W^* = -\dot{\mathbf{q}}^{*\mathbf{T}} \mathbf{M} \ddot{\mathbf{q}} \tag{12}$$

$$\mathbf{M_{3P}} = \rho \int_\Omega \mathbf{C}^\mathbf{T} \mathbf{C} d\Omega \tag{13}$$

Further development of the product of $\mathbf{C}^\mathbf{T}\mathbf{C}$ in Equation (13) yields to Equation (14).

$$\mathbf{M_{3P}} = \rho \int_\Omega \begin{bmatrix} c_e & 0 & c_f & 0 & c_g & 0 \\ 0 & c_e & 0 & c_f & 0 & c_g \\ c_f & 0 & c_h & 0 & c_i & 0 \\ 0 & c_f & 0 & c_h & 0 & c_i \\ c_g & 0 & c_i & 0 & c_j & 0 \\ 0 & c_g & 0 & c_i & 0 & c_j \end{bmatrix} d\Omega \tag{14}$$

with:

$$c_e = c_1^2 + 2c_1c_2 - 2c_1 + c_2^2 - 2c_2 + 1 \tag{15}$$

$$c_f = -c_1^2 - c_1c_2 + c_1 \tag{16}$$

$$c_g = -c_1c_2 - c_2^2 + c_2 \tag{17}$$

$$c_h = c_1^2 \tag{18}$$

$$c_i = c_1c_2 \tag{19}$$

$$c_j = c_2^2 \tag{20}$$

Note that Equation (14) involves solving the integrals of Equations (21)–(23).

$$\int_\Omega \rho d\Omega = m \tag{21}$$

$$\int_{\Omega} \rho \mathbf{c} d\Omega = \int_{\Omega} \rho \bar{\mathbf{X}}^{-1} \bar{\mathbf{r}} d\Omega = \rho \int_{\Omega} \begin{bmatrix} \frac{1}{l_{ij}} & -\frac{K_x}{K_y l_{ij}} \\ 0 & \frac{1}{K_y} \end{bmatrix} \begin{bmatrix} \bar{x} \\ \bar{y} \end{bmatrix} d\Omega = \rho \int_{\Omega} \begin{bmatrix} \frac{\bar{x}}{l_{ij}} - \frac{\bar{y} K_x}{K_y l_{ij}} \\ \frac{\bar{y}}{K_y} \end{bmatrix} d\Omega = \begin{bmatrix} \frac{m \bar{x}_g}{l_{ij}} - \frac{m \bar{y}_g K_x}{K_y l_{ij}} \\ \frac{m \bar{y}_g}{K_y} \end{bmatrix} \tag{22}$$

$$\int_{\Omega} \rho \mathbf{c}\mathbf{c}^{\mathbf{T}} d\Omega = \bar{\mathbf{X}}^{-1} \left(\int_{\Omega} \rho \bar{\mathbf{r}} \bar{\mathbf{r}}^{\mathbf{T}} d\Omega \right) \bar{\mathbf{X}}^{-\mathbf{T}} = \bar{\mathbf{X}}^{-1} \left(\int_{\Omega} \rho \begin{bmatrix} \bar{x}^2 & \bar{x}\bar{y} \\ \bar{x}\bar{y} & \bar{y}^2 \end{bmatrix} d\Omega \right) \bar{\mathbf{X}}^{-\mathbf{T}} = \bar{\mathbf{X}}^{-1} \begin{bmatrix} I_y & I_{xy} \\ I_{xy} & I_x \end{bmatrix} \bar{\mathbf{X}}^{-\mathbf{T}} = \begin{bmatrix} \frac{I_x K_x^2}{K_y^2 l_{ij}^2} - \frac{2 I_{xy} K_x}{K_y l_{ij}^2} + \frac{I_y}{l_{ij}^2} & -\frac{I_x K_x}{K_y^2 l_{ij}} + \frac{I_{xy}}{K_y l_{ij}} \\ -\frac{I_x K_x}{K_y^2 l_{ij}} + \frac{I_{xy}}{K_y l_{ij}} & \frac{I_x}{K_y^2} \end{bmatrix} \tag{23}$$

where m is the total mass of the element, $\bar{\mathbf{r}}$ represents the local coordinates of the center of gravity, and I_x, I_y, and I_{xy} are the moments and products of inertia with respect to local coordinates with origin at the basic point i.

By substituting the integrals of Equations (21)–(23) into Equation (14), we finally obtain the mass matrix $\mathbf{M_{3P}}$ (Equation (24)).

$$\mathbf{M_{3P}} = \begin{bmatrix} e & 0 & f & 0 & g & 0 \\ 0 & e & 0 & f & 0 & g \\ f & 0 & h & 0 & i & 0 \\ 0 & f & 0 & h & 0 & i \\ g & 0 & i & 0 & j & 0 \\ 0 & g & 0 & i & 0 & j \end{bmatrix} \tag{24}$$

with:

$$e = \frac{I_x K_x^2}{K_y^2 l^2} - \frac{2 I_x K_x}{K_y^2 l_{ij}} + \frac{I_x}{K_y^2} - \frac{2 I_{xy} K_x}{K_y l_{ij}^2} + \frac{2 I_{xy}}{K_y l_{ij}} + \frac{I_y}{l_{ij}^2} + \frac{2 K_x m \bar{y}_g}{K_y l_{ij}} + m - \frac{2 m \bar{x}_g}{l_{ij}} - \frac{2 m \bar{y}_g}{K_y} \tag{25}$$

$$f = -\frac{I_x K_x^2}{K_y^2 l_{ij}^2} + \frac{I_x K_x}{K_y^2 l_{ij}} + \frac{2 I_{xy} K_x}{K_y l_{ij}^2} - \frac{I_{xy}}{K_y l_{ij}} - \frac{I_y}{l_{ij}^2} - \frac{K_x m \bar{y}_g}{K_y l_{ij}} + \frac{m \bar{x}_g}{l_{ij}} \tag{26}$$

$$g = \frac{I_x K_x}{K_y^2 l_{ij}} - \frac{I_x}{K_y^2} - \frac{I_{xy}}{K_y l_{ij}} + \frac{m \bar{y}_g}{K_y} \tag{27}$$

$$h = \frac{I_x K_x^2}{K_y^2 l_{ij}^2} - \frac{2 I_{xy} K_x}{K_y l_{ij}^2} + \frac{I_y}{l_{ij}^2} \tag{28}$$

$$i = -\frac{I_x K_x}{K_y^2 l_{ij}} + \frac{I_{xy}}{K_y l_{ij}} \tag{29}$$

$$j = \frac{I_x}{K_y^2} \tag{30}$$

2.2. Six-Bar Mechanism

Figure 2 shows the six-bar mechanism. This kind of mechanism exhibits one degree of freedom and five mobile links.

Each of the links has a local coordinate system with its origin located at point i and the x axis directed toward point j. Each of the links has a mass m_{bn} and a center of gravity located at local coordinates (x_{bn}, y_{bn}) for $1 \leq n \leq 5$. The distribution of the points is detailed in Table 1.

For this mechanism, it is possible to define a vector $\mathbf{q}$ representing the positions of its basic points (Equation (31)).

$$\mathbf{q} = [A_x\ A_y\ B_x\ B_y\ C_x\ C_y\ D_x\ D_y\ E_x\ E_y\ F_x\ F_y\ G_x\ G_y]^T \tag{31}$$

By time-deriving $\mathbf{q}$, it is possible to obtain a new vector $\dot{\mathbf{q}}$ representing the velocities of each of the basic points of the mechanism (Equation (32)). Similarly, by time-deriving the velocity vector, the acceleration vector $\ddot{\mathbf{q}}$ can be obtained (Equation (33)).

$$\dot{\mathbf{q}} = [V_{Ax}\ V_{Ay}\ V_{Bx}\ V_{By}\ V_{Cx}\ V_{Cy}\ V_{Dx}\ V_{Dy}\ V_{Ex}\ V_{Ey}\ VFx\ V_{Fy}\ V_{Gx}\ V_{Gy}]^T \tag{32}$$

$$\ddot{\mathbf{q}} = [A_{Ax}\ A_{Ay}\ A_{Bx}\ A_{By}\ A_{Cx}\ A_{Cy}\ A_{Dx}\ A_{Dy}\ A_{Ex}\ A_{Ey}\ A_{Fx}\ A_{Fy}\ A_{Gx}\ A_{Gy}]^T \tag{33}$$

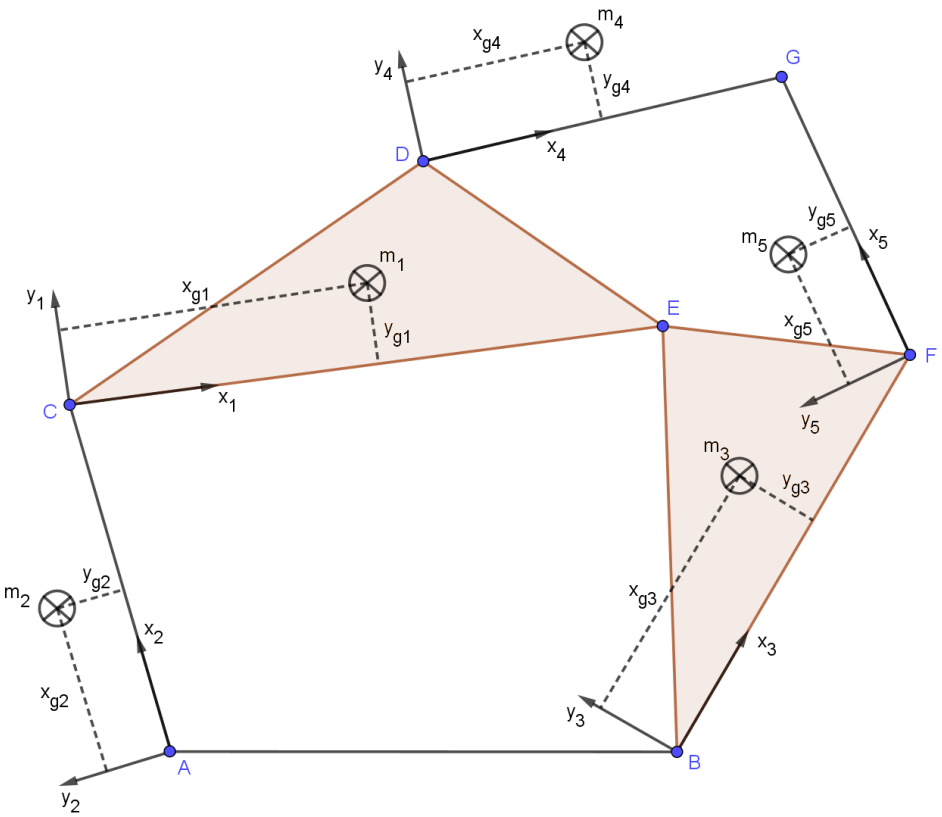

Figure 2. The six-bar mechanism.

Table 1. Point distribution for the six-bar mechanism.

Element	Point i	Point j	Point k
1	C	E	D
2	A	C	
3	B	F	E
4	D	G	
5	F	G	

2.3. Counterweight Addition

To proceed with the dynamic balancing of the six-bar mechanism, a set of cylindrical counterweights is added to its structure (Figure 3).

To simplify the procedure, let us assume that all counterweights are coincident with the basic point *i* of each of the elements of the mechanism. The center of gravity of each

counterweight is located at the local coordinates (x_{cn}, y_{cn}) for $1 \leq n \leq 5$. Their thickness is defined by t_{cn} for $1 \leq n \leq 5$.

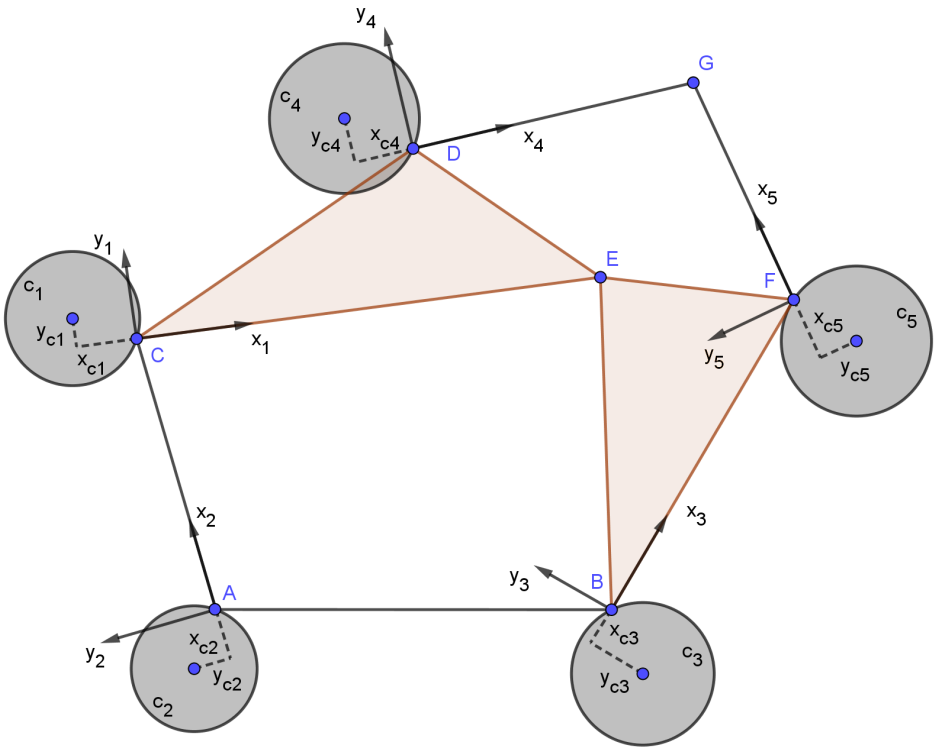

Figure 3. Six-bar mechanism with cylindrical counterweights.

It is then possible to define the mass m_{cn} of each counterweight as a function of its density $\rho_{cn} = \rho$, its thickness t_{cn}, and the location of its CoM (x_{cn}, y_{cn}), as shown in Equation (34).

$$m_{cn} = \rho\, V = \rho \pi t_{cn}(x_{cn}^2 + y_{cn}^2) \tag{34}$$

It is also possible to obtain the mass moments for each of the counterweights with respect to the local coordinate system origin, as shown in Equations (35) and (36).

$$I_{xcn} = \frac{1}{4} m_{cn}(x_{cn}^2 + y_{cn}^2) + m y_{cn}^2 = \frac{1}{4} m_{cn}(x_{cn}^2 + 5y_{cn}^2) = \frac{1}{4} \rho \pi t_{cn}(x_{cn}^2 + y_{cn}^2)(x_{cn}^2 + 5y_{cn}^2) \tag{35}$$

$$I_{ycn} = \frac{1}{4} m_{cn}(x_{cn}^2 + y_{cn}^2) + m x_{cn}^2 = \frac{1}{4} m_{cn}(5x_{cn}^2 + y_{cn}^2) = \frac{1}{4} \rho \pi t_{cn}(x_{cn}^2 + y_{cn}^2)(5x_{cn}^2 + y_{cn}^2) \tag{36}$$

The polar moment of inertia of each counterweight I_{zcn} with respect to the local coordinate system origin can be defined by Equation (37).

$$I_{zcn} = I_{xcn} + I_{ycn} = \frac{3}{2} m_{cn}(x_{cn}^2 + y_{cn}^2) = \frac{3}{2} \rho \pi t_{cn}(x_{cn}^2 + y_{cn}^2)^2 \tag{37}$$

Similarly, the product of inertia of each counterweight with respect to the local coordinate system origin can be calculated with Equation (38).

$$I_{xycn} = m_{cn} x_{cn} y_{cn} = \rho \pi t_{cn}(x_{cn}^2 + y_{cn}^2) x_{cn} y_{cn} \tag{38}$$

2.4. Mass Matrix for the Six-Bar Mechanism with Counterweights

To formulate the mass matrix of the balanced mechanism, it is necessary to obtain the mass matrices for each of the linkages (link and counterweight) first. The details of these individual mass matrices can be found in Appendix A.

Given that the mechanism consists of seven basic points, each of them represented by one (x, y) coordinate, the resulting mass matrix will consist of 14 columns and 14 rows.

Equation (39) shows the mass matrix M representing the six-bar mechanism with counterweights.

$$M = \begin{bmatrix}
a_2 & 0 & 0 & 0 & b_2 & c_2 & 0 & 0 & 0 & 0 & 0 & 0 & 0 & 0 \\
0 & a_2 & 0 & 0 & -c_2 & b_2 & 0 & 0 & 0 & 0 & 0 & 0 & 0 & 0 \\
0 & 0 & e_3 & 0 & 0 & 0 & 0 & 0 & g_3 & 0 & f_3 & 0 & 0 & 0 \\
0 & 0 & 0 & e_3 & 0 & 0 & 0 & 0 & 0 & g_3 & 0 & f_3 & 0 & 0 \\
b_2 & c_2 & 0 & 0 & d_2+e_1 & 0 & g_1 & 0 & f_1 & 0 & 0 & 0 & 0 & 0 \\
-c_2 & b_2 & 0 & 0 & 0 & d_2+e_1 & 0 & g_1 & 0 & f_1 & 0 & 0 & 0 & 0 \\
0 & 0 & 0 & 0 & g_1 & 0 & a_4+j_1 & 0 & i_1 & 0 & 0 & 0 & b_4 & c_4 \\
0 & 0 & 0 & 0 & 0 & g_1 & 0 & a_4+j_1 & 0 & i_1 & 0 & 0 & -c_4 & b_4 \\
0 & 0 & g_3 & 0 & f_1 & 0 & i_1 & 0 & h_1+i_3 & 0 & i_3 & 0 & 0 & 0 \\
0 & 0 & 0 & g_3 & 0 & f_1 & 0 & i_1 & 0 & h_1+i_3 & 0 & i_3 & 0 & 0 \\
0 & 0 & f_3 & 0 & 0 & 0 & 0 & 0 & i_3 & 0 & a_5+h_3 & 0 & b_5 & c_5 \\
0 & 0 & 0 & f_3 & 0 & 0 & 0 & 0 & 0 & i_3 & 0 & a_5+h_3 & -c_5 & b_5 \\
0 & 0 & 0 & 0 & 0 & 0 & b_4 & c_4 & 0 & 0 & b_5 & c_5 & d_4+d5 & 0 \\
0 & 0 & 0 & 0 & 0 & 0 & -c_4 & b_4 & 0 & 0 & -c_5 & b_5 & 0 & d_4+d_5
\end{bmatrix} \quad (39)$$

where $a_n, b_n, \ldots, j_n$ are the terms of the different mass matrices for linkages n = 1, …, 5 (see Appendix A).

2.5. Linear Momentum and Shaking Force

Once vectors $\mathbf{q}$, $\dot{\mathbf{q}}$, and $\ddot{\mathbf{q}}$ have been defined (Equations (31)–(33)), it is possible to calculate the linear momentum L associated to the balanced mechanism (Equation (40)).

$$\begin{bmatrix} L_i \\ L_j \end{bmatrix} = \mathbf{B}\mathbf{M}\dot{\mathbf{q}} \quad (40)$$

where $\mathbf{B}$ (Equation (41)) is a matrix formed by identity matrices matching the number of basic points in the mechanism.

$$\mathbf{B} = \begin{bmatrix} 1 & 0 & 1 & 0 & 1 & 0 & 1 & 0 & 1 & 0 & 1 & 0 & 1 & 0 \\ 0 & 1 & 0 & 1 & 0 & 1 & 0 & 1 & 0 & 1 & 0 & 1 & 0 & 1 \end{bmatrix}^{\mathbf{T}} \quad (41)$$

By solving Equation (40) and considering that the velocity of the fixed points is always zero ($VA_X = 0$, $VA_Y = 0$, $VB_X = 0$, $VB_Y = 0$), the expressions of the linear momentum ($\mathbf{L_i}$ and $\mathbf{L_j}$) can be obtained.

The ShF_i and ShF_j of the mechanism can be computed by time-deriving the equations $\mathbf{L_i}$ and $\mathbf{L_j}$ (Equation (40)) (expressions are not included in the paper because of their length).

To guarantee the equilibrium, the result of these derivatives must be constant (normally zero) in the analyzed period of time.

2.6. Angular Momentum and Shaking Moment

The use of FCC allows us to express the angular momentum H of the mechanim, as shown in Equation (42):

$$H = \mathbf{q} \times (\mathbf{M}\dot{\mathbf{q}}) = \mathbf{r}\mathbf{M}\dot{\mathbf{q}} \quad (42)$$

where $\mathbf{r}$ is given as a function of the basic points and can be expressed as Equation (43):

$$\mathbf{r} = \begin{bmatrix} -A_Y & A_X & -B_Y & B_X & -C_Y & C_X & -D_Y & D_X & -E_Y & E_X & -F_Y & F_X & -G_Y & G_X \end{bmatrix}^{\mathbf{T}} \quad (43)$$

The ShM can then be calculated by time-deriving H (Equations (44) and (45)).

$$ShM = \frac{dH}{dt} = \mathbf{r}\mathbf{M}\left(\frac{d(\dot{\mathbf{q}})}{dt}\right) + \left(\frac{d\mathbf{r}}{dt}\right)\mathbf{M}\dot{\mathbf{q}} \quad (44)$$

$$ShM = \frac{dH}{dt} = \mathbf{r}\mathbf{M}\ddot{\mathbf{q}} + \dot{\mathbf{r}}\mathbf{M}\dot{\mathbf{q}} \tag{45}$$

with:

$$\begin{aligned}\dot{\mathbf{r}} = [&-VA_Y \quad VA_X \quad -VB_Y \quad VB_X \quad -VC_Y \quad VC_X \quad -VD_Y \quad VD_X \\ &-VE_Y \quad VE_X \quad -VF_Y \quad VF_X \quad -VG_Y \quad VG_X]^{\mathbf{T}}\end{aligned} \tag{46}$$

To guarantee the dynamic equilibrium of the mechanism, the ShM must be constant, i.e., the time-derivative of H (Equation (45)) must be zero.

The ShM of the mechanism is finally obtained by solving Equation (45) and considering $VA_X = 0$, $VA_Y = 0$, $VB_X = 0$ y $VB_Y = 0$ (equation is not included in the paper because of its length).

3. Optimization

3.1. Objective Function

Two dimensionless balancing indexes β_i, containing the motion parameters ($\mathbf{q}$, $\dot{\mathbf{q}}$, and $\ddot{\mathbf{q}}$) of the six-bar mechanism, can be used to define the optimization's objective function: β_{ShF} and β_{ShM}.

β_{ShF} (Equation (47)) is defined by the RMS value of the ShF reaction of the optimized mechanism ($rms({}^oShF)$) with respect to the RMS value of the original mechanism ($rms(ShF)$), which are both considered over a time period T.

$$\beta_{ShF} = \frac{rms({}^oShF)}{rms(ShF)} = \sqrt{\frac{\sum_{k=1}^{N}({}^oShF_{ik}^2 + {}^oShF_{jk}^2)}{\sum_{k=1}^{N}(ShF_{ik}^2 + ShF_{jk}^2)}} \tag{47}$$

β_{ShM} (Equation (48)) can be calculated in a similar way. Nevertheless, the reaction produced by ShM must also be considered.

$$\beta_{ShM} = \frac{\sum_{k=1}^{N} {}^oShM_k^2}{\sum_{k=1}^{N} ShM_k^2} \tag{48}$$

where ${}^oShM$ is the shaking moment of the optimized mechanism and ShM is a constant representing the shaking moment of the unbalanced mechanism.

A multiobjective optimization problem emerges as it is desired to minimize both β_{ShF} and β_{ShM} considering the variables boundaries (i.e., the physical limits for the locations of the CoM (x_{cn} and y_{cn}) and the thickness (t_{cn}) of each counterweight). To solve this problem, a linear combination of the objectives is performed as proposed in Equation (49).

$$f(X) = \gamma * \beta_{ShM} + (1 - \gamma) * \beta_{ShF} \tag{49}$$

where γ is a scalar value that assigns the importance to each optimization objective. Thus, the 15 variables to be optimized are: $x_{c1}, y_{c1}, t_{c1}, x_{c2}, y_{c2}, t_{c2}, x_{c3}, y_{c3}, t_{c3}, x_{c4}, y_{c4}, t_{c4}, x_{c5}, y_{c5}$, and t_{c5}. The boundaries for optimization are defined according to Equation (50).

$$\begin{aligned} x_{cn}^{min} \leqslant x_{cn} \leqslant x_{cn}^{max} \\ y_{cn}^{min} \leqslant y_{cn} \leqslant y_{cn}^{max} \\ t_{cn}^{min} \leqslant t_{cn} \leqslant t_{cn}^{max} \end{aligned} \tag{50}$$

3.2. Algorithm

Once the objective function has been proposed, an optimization method can be applied. In this paper, we explore Differential Evolution (DE) [44].

Being an evolutionary algorithm, DE uses approaches inspired by the theory of evolution. It optimizes a problem by proposing a population of candidate solutions and creating new candidate solutions with the ones that obtained the best scores. Thus, the new gen-

erations are better than the previous ones. Recently, DE has been successfully applied to disruptive fields such as the oil market [45] and genome studies [46].

The DE algorithm proposed for the complete balancing optimization of the six-bar mechanism is presented in Algorithm 1. It was programmed in Python.

Algorithm 1: Differential Evolution (DE).

Input : $N = 255$, $F = 0.8$, $CR = 0.7$, $k_{max} = 100$

An initial population is generated $S = \{X_{1k}, X_{2k}, \ldots, X_{Nk}\}$
X_{best} = solution with the lowest value in the objective function
for $k = 0$ *until* k_{max} **do**
  $Q = \{\}$
  for $i = 1$ *until* N **do**
    Selection of three random solutions in S $\gamma, \delta, \eta \in \{1, \ldots, N\}, \gamma \neq \delta \neq \eta \neq i$
    $\hat{X}_{ik} = X_{\gamma k} + F(X_{\delta k} - X_{\eta k})$
    $\hat{X}_{ik} = Clip(\hat{X}_{ik})$
    for $j = 1$ *until* D **do**
      R = Random value between 0 and 1 with uniform distribution
      if $R \leq CR$ **then**
        $Y_{ikj} = \hat{X}_{ikj}$
      else
        $Y_{ikj} = X_{ikj}$
      end
    end
    if $f(Y_{ik}) < f(X_{ik})$ **then**
      $Q = Q \cup Y_{ik}$
    else
      $Q = Q \cup X_{ik}$
    end
    If $f(Y_{ik}) < f(X_{best})$ **then** $X_{best} = Y_{ik}$
  end
  $S = Q$
  $k = k + 1$
end
return X_{best}

Given that the number of variables to optimize is equal to 15, a population of $N = 15^2 = 225$ solutions is created, identifying the n_{th} solution of generation k with the vector X_{Nk}. Solutions are initialized following a uniform distribution bounded by limits between the allowed ranges for each variable. Three solutions are then selected to perform the random mutation: $X_{\gamma k}$, $X_{\delta k}$, and $X_{\eta k}$ to generate a new solution: $\hat{X}_{ik} = X_{\gamma k} + F(X_{\delta k} - X_{\eta k})$ with F being a random value between 0 and 2.

The crossover is performed with a probability $CR = 0.7$. Then, Y_{ik} and X_{ik} are evaluated in the function to be optimized. To be considered part of the new generation, the one with the best results is chosen. The generations are repeated 100 times, resulting in the solution exhibiting the lowest value.

4. Results

This section presents the numerical results of the dynamic balancing of the six-bar mechanism with FCC and DE optimization. To better visualize the influence of the counterweights on the procedure, a Pareto front analysis is proposed. This tool allows to restrict our attention to the set of best solutions and ease the decision-making process.

Table 2 summarizes the physical parameters of the six-bar mechanism shown in Figure 2. Steel links have been considered with a density of 7800 kg/m^3. The counterweights are considered to be made of brass with a density ρ_{cn} = 8500 kg/m^3.

Table 2. Parameters of the six-bar mechanism used in the example. Those indicated with a '-' are not necessary for the numerical analysis.

Link n	**1**	**2**	**3**	**4**	**5**
Mass m_{b_n} [kg]	0.6935	0.1022	0.9636	0.1825	0.1679
Length l_n [m]	0.19	0.14	0.13416408	0.25	0.23
Inertia I_{xb_n} [kg m/s^2]	0.00116161	-	0.00622646	-	-
Inertia I_{yb_n} [kg m/s^2]	0.00556534	-	0.00657336	-	-
Inertia I_{zb_n} [kg m/s^2]	-	0.00066856	-	0.00380360	0.00296204
Inertia I_{xyb_n} [kg m/s^2]	0.00167596	-	0.00522914	-	-
CoM x_{b_n} [m]	0.08	0.07	0.07751702	0.125	0.115
CoM y_{b_n} [m]	0.03333333	0.0	0.06559133	0.0	0.0
K_x [m]	0.05	-	0.09838699	-	-
K_y [m]	0.1	-	0.196677398	-	-

A motor located at point A is responsible for actuating the mechanism. Its rotating speed has been fixed at 500 rpm. Using direct kinematics, it is possible to obtain a sample of the positions, velocities, and accelerations at each of the basic points of the mechanism.

By replacing all known parameters in the equations of the balancing indexes (Equations (47) and (48)), it is possible to define the objective function (Equation (49)). According to the mechanical characteristics of this particular example, the boundaries considered for the optimization are shown in Equation (51):

$$\begin{aligned} -0.16\,\text{m} \leqslant x_{cn}, y_{cn} \leqslant 0.16\,\text{m} \\ 0.005\,\text{m} \leqslant t_{cn} \leqslant 0.04\,\text{m} \end{aligned} \tag{51}$$

4.1. Optimization with Five Counterweights

The DE algorithm was executed until 200 valid solutions (i.e., solutions resulting from the objective function optimization with values between 0 and 1) were obtained considering γ as a random value with uniform distribution in the range (0, 1), following the random search of the hyper-parameters presented in [47].

Figure 4a shows the relationship between the β_{ShF} and the β_{ShM} values for all the solutions found. Different colors are used to represent the values used for γ in the objective function f(X) (Equation (49)).

In Figure 4b, the dark points represent the Pareto front while the light ones represent the dominated solutions.

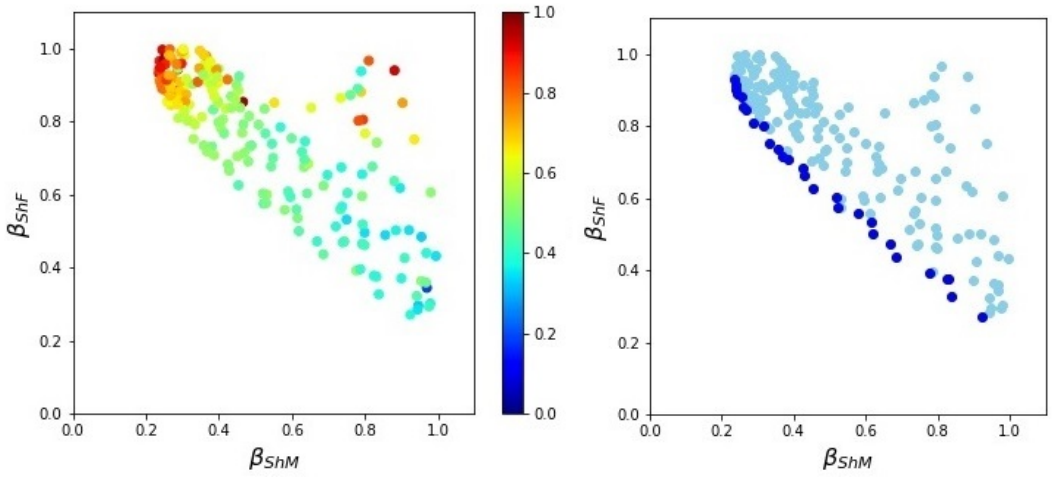

(**a**) (**b**)

Figure 4. Pareto analysis of the optimization objectives: β_{ShM} and β_{ShF}. (**a**) Optimized β_{ShM} and β_{ShF} according to γ. (**b**) Pareto Front of the optimized objectives.

Among all the solutions found in the Pareto front, it is possible to select the one that is the most appropriate according to the desired type of balancing. To exemplify this statement, let us consider three different solutions from the Pareto front.

In the first one, a greater importance is given to balancing the ShM (β_{ShM}= 0.235917108, β_{ShF} = 0.932850297). In the second one, a greater importance is given to balancing the ShF (β_{ShM} = 0.924195224, β_{ShF} = 0.270900009). Finally, in the third solution, the same importance is given to balancing both the ShF and ShM (β_{ShM} = 0.580111266, β_{ShF} = 0.558041831). These solutions are detailed below.

1. In the first solution, a greater importance is given to balancing the ShM. This is achieved by choosing the minimum value of index β_{ShM} (β_{ShM} = 0. 235917108), which allows us to obtain an improvement of 76.4% without considering any improvement of the ShF (β_{ShF} = 0.932850297). The following variables values correspond to this solution:

$$\begin{array}{lll} x_{c1} = -0.02611622 & y_{c1} = -0.033186164 & t_{c1} = 0.021370695 \\ x_{c2} = -0.06 & y_{c2} = -0.012314794 & t_{c2} = 0.039459546 \\ x_{c3} = -0.06 & y_{c3} = 0.016752092 & t_{c3} = 0.039814955 \\ x_{c4} = -0.002045161 & y_{c4} = -0.000151565 & t_{c4} = 0.005 \\ x_{c5} = 0.001614171 & y_{c5} = 0.00639164 & t_{c5} = 0.005106848 \end{array}$$

2. The second chosen solution in the Pareto front is the one with the minimum value in β_{ShF} (β_{ShF} = 0.270900009), which achieves an improvement of 72.91% in balancing the ShM. This choice assigns no importance to the balancing of the ShM (β_{ShM} = 0.924195224). This solution yields to the following variable values:

$$\begin{array}{lll} x_{c1} = -0.049437705 & y_{c1} = -0.04279353 & t_{c1} = 0.0074319 \\ x_{c2} = -0.06 & y_{c2} = -0.001485936 & t_{c2} = 0.038953174 \\ x_{c3} = -0.050813691 & y_{c3} = -0.017724236 & t_{c3} = 0.039660979 \\ x_{c4} = 0.001669535 & y_{c4} = 0.005996916 & t_{c4} = 0.005 \\ x_{c5} = 0.000387207 & y_{c5} = 0.013090811 & t_{c5} = 0.005 \end{array}$$

3. The third chosen solution is the one in the Pareto front where both indexes are optimized (β_{ShM} = 0.580111266, β_{ShF} = 0.558041831). By using this solution, the ShM is reduced by 41.99% and the ShF is reduced by 44.2%. It corresponds to the following variable values:

$$
\begin{array}{lll}
x_{c1} = -0.06 & y_{c1} = -0.030069707 & t_{c1} = 0.006021448 \\
x_{c2} = -0.06 & y_{c2} = -0.00383543 & t_{c2} = 0.04 \\
x_{c3} = -0.06 & y_{c3} = 0.004650961 & t_{c3} = 0.028206906 \\
x_{c4} = 0.000606455 & y_{c4} = -0.001322538 & t_{c4} = 0.005416754 \\
x_{c5} = 0.000545683 & y_{c5} = -0.0000185 & t_{c5} = 0.005
\end{array}
$$

To measure the method's efficiency, we assessed two parameters: convergence and computing time. Figure 5 shows the process of convergence of the objective function $f(X)$ as a function of generations. Six executions are presented with different γ values. Note that all executions exhibit values higher than 1.0 at the beginning of the execution (i.e., not optimized at all). After the 40th generation, all reach convergence (the closer the value to zero, the better), proving that the DE method actually optimizes the objective function.

Computing time is a major concern in the efficiency of optimization algorithms. To measure it, we executed 50 times the DE optimization procedure on a desktop computer with an Intel Core i7 processor (2.40 GHz), 8 GB RAM, and Windows 10 OS. The average computing time was 15.22 min with a standard deviation of 0.25 min. Being a mechanical design application, the optimization procedure does not require a fast or real-time computing but rather a practical one.

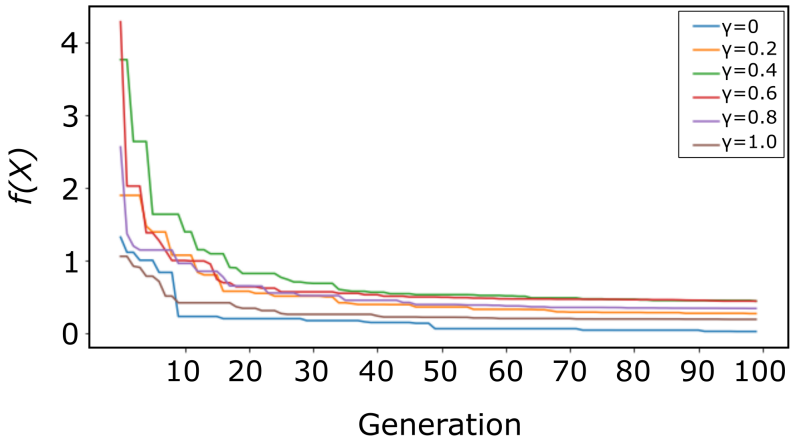

Figure 5. The convergence of the objective function $f(X)$ with the DE method.

4.2. Dimensions of the Counterweights

An analysis is now presented to determine if the proposed boundaries for the optimization are the most suitable or if they should be modified (in case there is the possibility of changing them due to the mechanical constraints of the mechanism and its surrounding space).

Figure 6 shows the box plots of the partial derivatives of the objective function with respect to each of the variables to be optimized x_n, y_n, and t_n for each of the n counterweights $(1 \leq n \leq 5)$ when evaluated at the optimal solutions.

We can state that optimal boundaries have been found when all the values of the partial derivatives of the objective function are close to zero. In the box plots of Figure 6, it can be seen that the partial derivatives of the variables $x_1, y_1, y_2, y_3, x_4, y_4, t_4, x_5, y_5$, and t_5 are close to zero, implying that the proposed boundaries allow such variables to reach their optimal values.

However, note that variables t_1, x_2, t_2, x_3, and t_3 have partial derivative values that are not close to zero. For example, in t_1 and even more significantly in x_2 and x_3, the values tend to be greater than zero; hence, it can be deduced that better optimization results could be obtained if: (1) the thicknesses of counterweight 1 were smaller than the fixed boundary of 0.005 m (i.e., practically eliminating counterweight 1) and (2) the x-axis positions of counterweights 1 and 3 were less than the limit of -0.16 m (i.e., moving their CoM in their –x local axis).

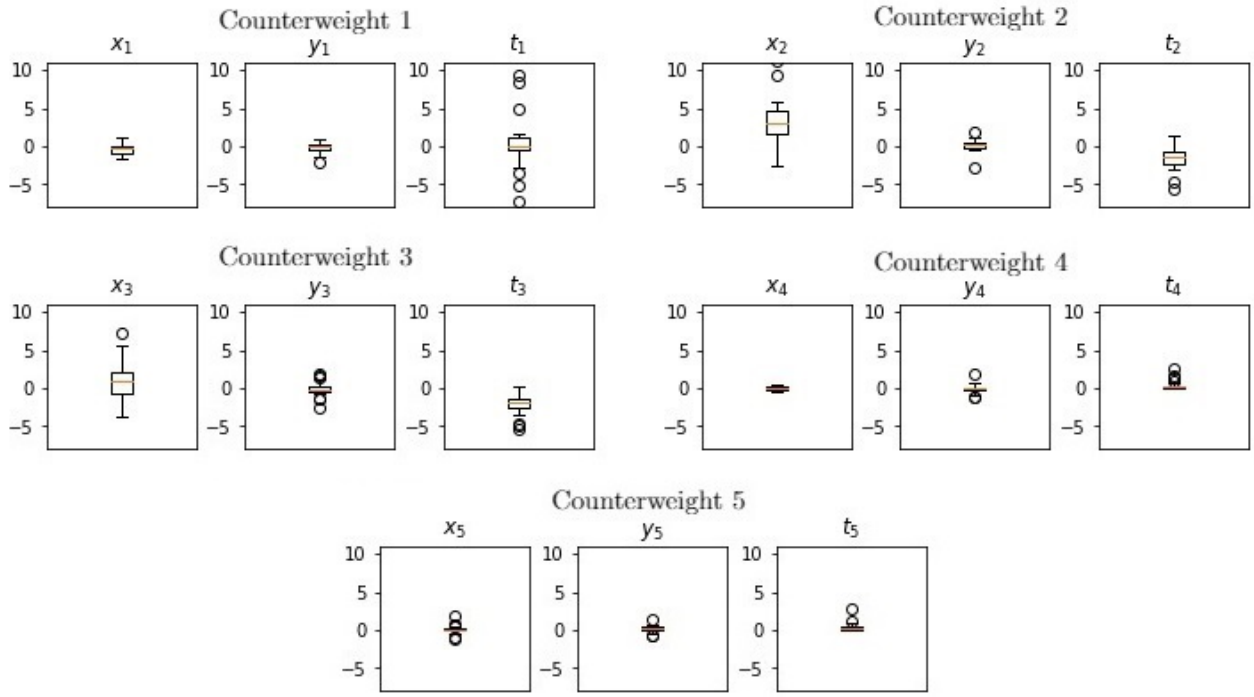

Figure 6. Box plots of partial derivatives of the objective function with respect to each optimization variable when using five counterweights.

On the other hand, the values of the partial derivatives of variables t_2 and t_3 tend to be less than zero, which means that, if possible, it would be convenient to further extend the boundaries of the optimization of these variables to values greater than 0.04 m.

Note that the information obtained from the Pareto front of the partial derivatives of the objective function is extremely useful to make decisions concerning the boundaries of the optimization, allowing us to foresee pertinent changes in the linkages as far as their mechanical conditions allow it.

Figure 7a shows the histograms of the volumes of the counterweights obtained from the different optimization results. Together with the analysis of the counterweights' area and thickness shown in Figure 7b, it is possible to conclude that counterweight 4 can be eliminated: it has a very small volume compared to the other counterweights, and its thickness and area are practically negligible.

In addition, for both counterweights 2 and 3, it can be appreciated that their thickness tends to remain at the upper limit of the optimization, thus confirming the result of the partial derivatives analysis: if the mechanical characteristics of the mechanism allow it, it would be advisable to extend the upper limit of their thicknesses.

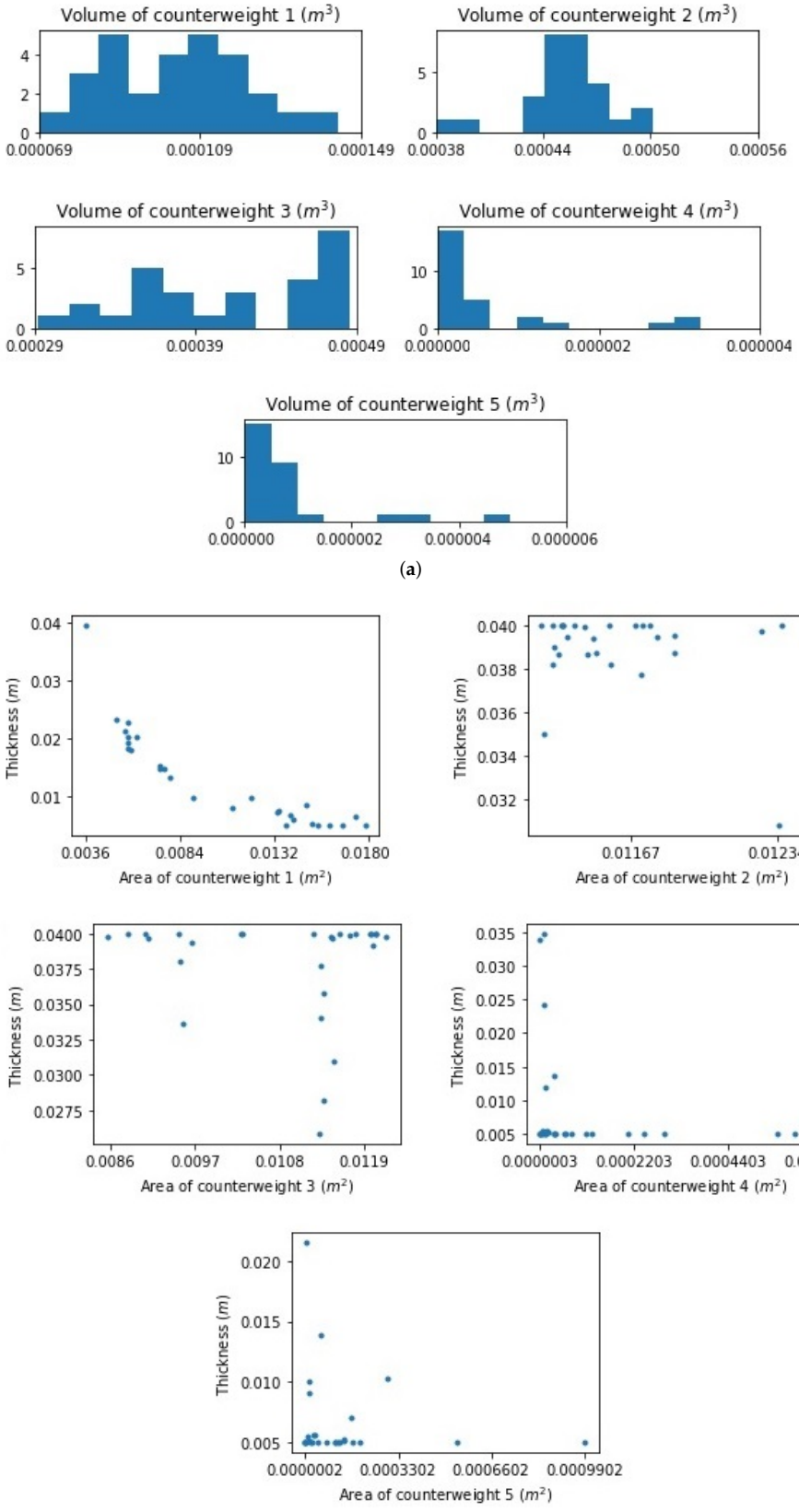

(**a**)

(**b**)

Figure 7. Dimensional analysis for the five counterweights balancing the six-bar mechanism. (**a**) Volumes of the five counterweights. (**b**) Relationship between the area and the thickness for the five counterweights.

4.3. Implementation

The optimization method and the dimensional analysis conclude with the design of a solution that effectively reduces the dynamic reactions of the six-bar mechanism.

Let us consider the third case where both ShF and ShM are optimized. Figure 8 shows the proposed implementation. As suggested by the analysis, counterweight 4 has been eliminated. Note that counterweight 5 is not visible because it exhibits very small dimensions in relation to the mechanism. Yet, it has been considered for the dynamic balancing of the mechanism.

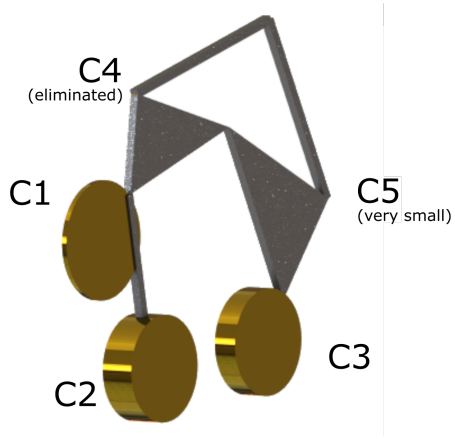

Figure 8. Conceptual implementation of the third solution from the Pareto front for the six-bar mechanism using five counterweights C_i.

4.4. Optimization with Four or Less Counterweights

The previous analysis suggested that not all five counterweights are strictly needed to balance the six-bar mechanism: counterweight 4 is meaningless and counterweight 5 is so small that it can be practically eliminated. When seeking a simple solution, i.e., one that does not involve adding too much volume to the mechanism, it may be useful to reduce the number of counterweights as long as they still provide acceptable results.

We performed the same analysis for four, three, two, and one counterweights. Figure 9 shows a comparison between the Pareto fronts of the different optimization results as a function of the number of counterweights. Note that as expected, similar results are obtained when using five, four, and three counterweights. So, a general conclusion for the implementation would be to use three counterweights.

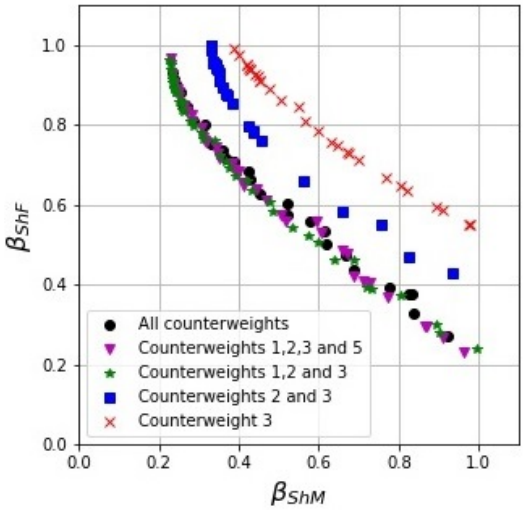

Figure 9. Pareto front comparison of the optimization objectives β_{ShM} and β_{ShF} according to the number of counterweights.

Table 3 summarizes the results obtained. The best results are highlighted in blue. Again, the best choice depends on the desired balancing: only the ShF, only the ShM, or both.

Table 3. Summary of the optimization results for the six-bar mechanism balancing.

Counterweights Cn	ShF Optimization % ShF, % ShM	ShM Optimization % ShF, % ShM	ShF and ShM Optimization % ShF, % ShM
All 5	72.91, 7.59	6.72, 76.41	44.2, 41.99
C1, C2, C3, C4	**76.82, 3.59**	3.21, 76.97	44.31, 40.73
C1, C2, C3	75.95, 0.5	**3.53, 77.21**	**45.69, 46.81**
C2, C3	56.98, 6.52	0.17, 67	41.66, 34.18
C3	44.97, 2.26	1.03, 61	28.69, 30.23

5. Discussion

The implementation of well-designed counterweights allows us to reduce the ShF and ShM by 76.82% and 77.21%, respectively, when importance is given to either of them and by 45.69% and 46.81%, respectively, when equal importance is given to both of them.

Table 4 compares our balancing results with others previously reported in the literature. Note that the comparison is limited to the cases where either the ShF or the ShM are optimized as not all the studies report the joint optimization. Table 4 includes other types of mechanisms such as the crank-slider and the four-bar mechanism, which are indeed simpler structures and thus easier to optimize. Six-bar mechanisms and their balancing are more complex and less frequently found in the literature because, as explained in Section 2, they exhibit a higher number of links with some defined by three basic points.

Table 4. Comparison of balancing results for several types of mechanisms and optimization methods.

Reference, CC or FCC	Mechanism	Optimization Algorithm	% of ShF Optimization	% of ShM Optimization
[48], CC	crank-slider	Differential Evolution	61.42	65.96
[49], CC	crank-slider	Teaching–Learning	48	44
[50], CC	crank-slider	Genetic	46	99
[51], **FCC**	**crank-slider**	**Differential Evolution**	**97.76**	**94.58**
[52], CC	four-bar	Genetic	50	68
[36], CC	four-bar	Firefly	86.3	83.39
[38], **FCC**	**four-bar**	**Gradient Descent**	**99.70**	**83.99**
[53], CC	six-bar	Genetic	48.5	32.35
This work, FCC	**six-bar**	**Differential Evolution**	**76.82**	**77.21**

Note that the use of FFC to define the mass matrix of a mechanism and thus obtain the expressions representing the dynamic reactions in its base, in conjunction with an optimization algorithm, is a suitable methodology for the complete balancing of mechanisms. Our previous work in crank-sliders [51] and four-bar [38] mechanisms confirm the efficiency of the proposed approach. The results obtained surpass those of approaches using Cartesian coordinates (CC).

The DE optimization method was successfully applied to solve the balancing problem of a six-bar mechanism. DE is a simple yet robust approach to address multiobjective problems.

Comparison between Pareto fronts has proven to be a useful tool for better visualizing the impact of each counterweight on the dynamic balancing of the mechanism.

The effectiveness of the analysis of the boundaries by means of box plots of the partial derivatives of the variables to be optimized together with the histograms of volumes and relations between area and thickens were also demonstrated. They ease the visualization of possible improvements on the counterweights and allow us to make useful decisions on their implementation.

Balancing six-bar mechanisms is highly appreciated in areas such as mobile robotics, since this type of linkage is used in humanoid robots [54] and bionic legs [55,56] as well as in rehabilitation engineering [57], in which balancing could minimize the reactions caused by the devices' motion, thus improving their performance and usability.

6. Conclusions

This paper has presented a novel approach for the complete (or dynamic) balancing of mechanisms: the use of fully Cartesian coordinates (FCC) in conjunction with an optimization method such as Differential Evolution (DE).

Among the main contributions of this paper is the development of the two-dimensional mass matrix for elements defined by three basic points. To our knowledge, this matrix has not been proposed so far in the literature and it can be applied to a vast number of more complex mechanisms that use type of linkages. By using FCC, this work has demonstrated that even for the most complex mechanisms, it is possible to obtain relatively simple non-trigonometric equations that define the ShF and ShM and to further optimize their dynamic balancing with algorithms such as DE with very good results.

As future work, it is expected to continue exploring FCC together with other metaheuristic methods to optimize more complex mechanisms in two and three dimensions. Our approach promises to be highly efficient for optimizing the balancing conditions of even more complex mechanisms once their mass matrices have been defined.

Author Contributions: Conceptualization, M.A. and M.T.O.-G.; methodology, M.T.O.-G. and C.N.S.; simulation, M.T.O.-G.; validation, D.U.C.-D., P.V. and R.V.; formal analysis, M.A., R.V. and A.A.G.; investigation, M.T.O.-G., M.A. and R.V.; writing—original draft preparation, M.T.O.-G.; writing—review and editing, R.V. and P.V.; visualization, D.U.C.-D. and A.A.G.; supervision, M.A. and R.V. All authors have read and agreed to the published version of the manuscript.

Funding: This research received no external funding.

Institutional Review Board Statement: Not applicable.

Informed Consent Statement: Not applicable.

Conflicts of Interest: The authors declare no conflict of interest.

Abbreviations

The following abbreviations are used in this manuscript:

CC	Cartesian Coordinates
FCC	Fully Cartesian Coordinates
ShF	Shaking Force
ShM	Shaking Moment
CoM	Center of Mass
DE	Differential Evolution

Appendix A. Mass-Matrix for Individual Linkages

It is necessary to define the mass matrix for each of the linkages in order to assemble the mass matrix of the entire mechanism.

Given that each counterweight is firmly attached to its corresponding link and that their position with respect to the local reference system does not change with the mechanism's motion, it is possible to consider five linkages to be optimized, each of them encompassing a link and a counterweight.

Linkages 1 and 3 have mass matrices consisting of three basic points, while linkages 2, 4, and 5 have mass matrices involving two basic points.

To define the different mass matrices, it is necessary to substitute the terms m, $\bar{x}_g$, $\bar{y}_g$, I_x, I_y, I_{xy}, and I_z in the equations that define the mass matrices of two and three points,

considering the contribution of both the link and the counterweight. Thus, for each n linkage, Equations (A1)–(A7) can be written.

$$m_n = m_{bn} + m_{cn} = m_{bn} + \rho\pi t_{cn}(x_{cn}^2 + y_{cn}^2) \tag{A1}$$

$$x_{gn} = \frac{x_{bn}m_{bn} + x_{cn}m_{cn}}{m_{bn} + m_{cn}} \tag{A2}$$

$$y_{gn} = \frac{y_{bn}m_{bn} + y_{cn}m_{cn}}{m_{bn} + m_{cn}} \tag{A3}$$

$$I_{xn} = I_{xbn} + I_{xcn} = I_{xbn} + \frac{1}{4}\rho\pi t_{cn}(x_{cn}^2 + y_{cn}^2)(x_{cn}^2 + 5y_{cn}^2) \tag{A4}$$

$$I_{yn} = I_{ybn} + I_{ycn} = I_{ybn} + \frac{1}{4}\rho\pi t_{cn}(x_{cn}^2 + y_{cn}^2)(5x_{cn}^2 + y_{cn}^2) \tag{A5}$$

$$I_{xyn} = I_{xybn} + I_{xycn} = I_{xybn} + \rho\pi t_{cn}(x_{cn}^2 + y_{cn}^2)x_{cn}y_{cn} \tag{A6}$$

$$I_{zn} = I_{zbn} + I_{zcn} = I_{xbn} + I_{ybn} + I_{xcn} + I_{ycn} \tag{A7}$$

Appendix A.1. Mass Matrix for Linkages 1 and 3

To define the mass matrix of linkage 1, let us consider point C as i, point E as j, and point D as k. Similarly, for linkage 3, point B is considered as i, point F as j, and point E as k.

Figure A1 shows the distances K_{x1}, K_{y1}, K_{x3}, and K_{y3}. Note that for linkage 1, $l_{ij} = l_1$ corresponds to the distance $\bar{CE}$ while for linkage 2, $l_{ij} = l_2$ corresponds to the distance $\bar{BF}$.

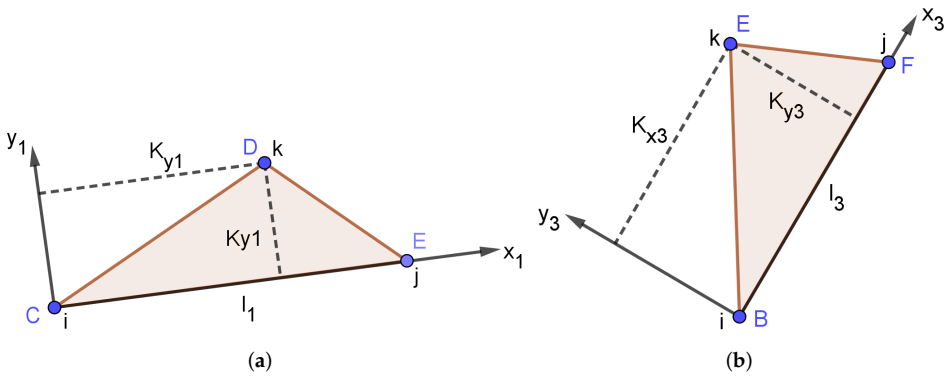

Figure A1. Linkages defined by three basic points. (**a**) Linkage 1. (**b**) Linkage 3.

By using the mass matrix $\mathbf{M_{3P}}$ (Equation (24)), the terms of the mass matrix for linkages $n = 1$ and $n = 3$ can be defined according to Equations (A8)–(A13).

$$
\begin{aligned}
e_n =& \frac{I_{xbn}K_{xn}^2}{K_{yn}^2 l_n^2} - \frac{2I_{xbn}K_{xn}}{K_{yn}^2 l_n} + \frac{I_{xbn}}{K_{yn}^2} - \frac{2I_{xybn}K_{xn}}{K_{yn}l_n^2} + \frac{2I_{xybn}}{K_{yn}l_n} + \frac{I_{ybn}}{l_n^2} + \frac{\pi K_{xn}^2\rho_{cn}t_{cn}x_{cn}^4}{4K_{yn}^2 l_n^2} \\
&+ \frac{3\pi K_{xn}^2\rho_{cn}t_{cn}x_{cn}^2}{2K_{yn}^2 l_n^2}y_{cn}^2 + \frac{5\pi K_{xn}^2\rho_{cn}t_{cn}y_{cn}^4}{4K_{yn}^2 l_n^2} + \frac{2K_{xn}m_{bn}y_{bn}}{K_{yn}l_n} + \frac{2\pi K_{xn}\rho_{cn}}{K_{yn}l_n}t_{cn}x_{cn}^2 y_{cn} \\
&+ \frac{2\pi K_{xn}\rho_{cn}}{K_{yn}l_n}t_{cn}y_{cn}^3 - \frac{2\pi K_{xn}\rho_{cn}}{K_{yn}l_n^2}t_{cn}x_{cn}^3 y_{cn} - \frac{2\pi K_{xn}\rho_{cn}}{K_{yn}l_n^2}t_{cn}x_{cn}y_{cn}^3 - \frac{\pi K_{xn}\rho_{cn}t_{cn}x_{cn}^4}{2K_{yn}^2 l_n} \\
&- \frac{3\pi K_{xn}\rho_{cn}}{K_{yn}^2 l_n}t_{cn}x_{cn}^2 y_{cn}^2 - \frac{5\pi K_{xn}\rho_{cn}t_{cn}y_{cn}^4}{2K_{yn}^2 l_n} - \frac{2m_{bn}^2 x_{bn}}{l_n m_{bn} + \pi l_n\rho_{cn}t_{cn}x_{cn}^2 + \pi l_n\rho_{cn}t_{cn}y_{cn}^2} \\
&- \frac{2m_{bn}^2 y_{bn}}{K_{yn}m_{bn} + \pi K_{yn}\rho_{cn}t_{cn}x_{cn}^2 + \pi K_{yn}\rho_{cn}t_{cn}y_{cn}^2} - \frac{2\pi m_{bn}\rho_{cn}t_{cn}x_{bn}x_{cn}^2}{l_n m_{bn} + \pi l_n\rho_{cn}t_{cn}x_{cn}^2 + \pi l_n\rho_{cn}t_{cn}y_{cn}^2} \\
&- \frac{2\pi m_{bn}\rho_{cn}t_{cn}x_{bn}y_{cn}^2}{l_n m_{bn} + \pi l_n\rho_{cn}t_{cn}x_{cn}^2 + \pi l_n\rho_{cn}t_{cn}y_{cn}^2} - \frac{2\pi m_{bn}\rho_{cn}t_{cn}x_{cn}^3}{l_n m_{bn} + \pi l_n\rho_{cn}t_{cn}x_{cn}^2 + \pi l_n\rho_{cn}t_{cn}y_{cn}^2} \\
&- \frac{2\pi m_{bn}\rho_{cn}t_{cn}x_{cn}^2 y_{bn}}{K_{yn}m_{bn} + \pi K_{yn}\rho_{cn}t_{cn}x_{cn}^2 + \pi K_{yn}\rho_{cn}t_{cn}y_{cn}^2} \\
&- \frac{2\pi m_{bn}\rho_{cn}t_{cn}x_{cn}^2 y_{cn}}{K_{yn}m_{bn} + \pi K_{yn}\rho_{cn}t_{cn}x_{cn}^2 + \pi K_{yn}\rho_{cn}t_{cn}y_{cn}^2} \\
&- \frac{2\pi m_{bn}\rho_{cn}t_{cn}x_{cn}y_{cn}^2}{l_n m_{bn} + \pi l_n\rho_{cn}t_{cn}x_{cn}^2 + \pi l_n\rho_{cn}t_{cn}y_{cn}^2} - \frac{2\pi m_{bn}\rho_{cn}t_{cn}y_{bn}y_{cn}^2}{K_{yn}m_{bn} + \pi K_{yn}\rho_{cn}t_{cn}x_{cn}^2 + \pi K_{yn}\rho_{cn}t_{cn}y_{cn}^2} \\
&- \frac{2\pi m_{bn}\rho_{cn}t_{cn}y_{cn}^3}{K_{yn}m_{bn} + \pi K_{yn}\rho_{cn}t_{cn}x_{cn}^2 + \pi K_{yn}\rho_{cn}t_{cn}y_{cn}^2} - \frac{2\pi^2\rho_{cn}^2 t_{cn}^2 x_{cn}^5}{l_n m_{bn} + \pi l_n\rho_{cn}t_{cn}x_{cn}^2 + \pi l_n\rho_{cn}t_{cn}y_{cn}^2} \\
&- \frac{2\pi^2\rho_{cn}^2 t_{cn}^2 x_{cn}^4 y_{cn}}{K_{yn}m_{bn} + \pi K_{yn}\rho_{cn}t_{cn}x_{cn}^2 + \pi K_{yn}\rho_{cn}t_{cn}y_{cn}^2} - \frac{4\pi^2\rho_{cn}^2 t_{cn}^2 x_{cn}^3 y_{cn}^2}{l_n m_{bn} + \pi l_n\rho_{cn}t_{cn}x_{cn}^2 + \pi l_n\rho_{cn}t_{cn}y_{cn}^2} \\
&- \frac{4\pi^2\rho_{cn}^2 t_{cn}^2 x_{cn}^2 y_{cn}^3}{K_{yn}m_{bn} + \pi K_{yn}\rho_{cn}t_{cn}x_{cn}^2 + \pi K_{yn}\rho_{cn}t_{cn}y_{cn}^2} - \frac{2\pi^2\rho_{cn}^2 t_{cn}^2 x_{cn}y_{cn}^4}{l_n m_{bn} + \pi l_n\rho_{cn}t_{cn}x_{cn}^2 + \pi l_n\rho_{cn}t_{cn}y_{cn}^2} \\
&- \frac{2\pi^2\rho_{cn}^2 t_{cn}^2 y_{cn}^5}{K_{yn}m_{bn} + \pi K_{yn}\rho_{cn}t_{cn}x_{cn}^2 + \pi K_{yn}\rho_{cn}t_{cn}y_{cn}^2} + 1 + \frac{5\pi\rho_{cn}t_{cn}}{4l_n^2}x_{cn}^4 + \frac{3\pi\rho_{cn}t_{cn}}{2l_n^2}x_{cn}^2 y_{cn}^2 \\
&+ \frac{\pi\rho_{cn}t_{cn}y_{cn}^4}{4l_n^2} + \frac{2\pi\rho_{cn}t_{cn}}{K_{yn}l_n}x_{cn}^3 y_{cn} + \frac{2\pi\rho_{cn}t_{cn}}{K_{yn}l_n}x_{cn}y_{cn}^3 + \frac{\pi\rho_{cn}t_{cn}x_{cn}^4}{4K_{yn}^2} + \frac{3\pi\rho_{cn}t_{cn}}{2K_{yn}^2}x_{cn}^2 y_{cn}^2 \\
&+ \frac{5\pi\rho_{cn}t_{cn}}{4K_{yn}^2}y_{cn}^4
\end{aligned}
\tag{A8}
$$

$$
\begin{aligned}
f_n =& -\frac{I_{xbn}K_{xn}^2}{K_{yn}^2 l_n^2} + \frac{I_{xbn}K_{xn}}{K_{yn}^2 l_n} + \frac{2I_{xybn}K_{xn}}{K_{yn}l_n^2} - \frac{I_{xybn}}{K_{yn}l_n} - \frac{I_{ybn}}{l_n^2} - \frac{\pi K_{xn}^2\rho_{cn}t_{cn}x_{cn}^4}{4K_{yn}^2 l_n^2} \\
&- \frac{3\pi K_{xn}^2\rho_{cn}t_{cn}x_{cn}^2}{2K_{yn}^2 l_n^2}y_{cn}^2 - \frac{5\pi K_{xn}^2\rho_{cn}t_{cn}y_{cn}^4}{4K_{yn}^2 l_n^2} - \frac{K_{xn}m_{bn}y_{bn}}{K_{yn}l_n} - \frac{\pi K_{xn}\rho_{cn}t_{cn}}{K_{yn}l_n}x_{cn}^2 y_{cn} \\
&- \frac{\pi K_{xn}\rho_{cn}t_{cn}}{K_{yn}l_n}y_{cn}^3 + \frac{2\pi K_{xn}\rho_{cn}}{K_{yn}l_n^2}t_{cn}x_{cn}^3 y_{cn} + \frac{2\pi K_{xn}\rho_{cn}}{K_{yn}l_n^2}t_{cn}x_{cn}y_{cn}^3 + \frac{\pi K_{xn}\rho_{cn}t_{cn}x_{cn}^4}{4K_{yn}^2 l_n} \\
&+ \frac{3\pi K_{xn}\rho_{cn}t_{cn}x_{cn}^2}{2K_{yn}^2 l_n}y_{cn}^2 + \frac{5\pi K_{xn}\rho_{cn}t_{cn}y_{cn}^4}{4K_{yn}^2 l_n} + \frac{m_{bn}x_{bn}}{l_n} + \frac{\pi\rho_{cn}}{l_n}t_{cn}x_{cn}^3 + \frac{\pi\rho_{cn}}{l_n}t_{cn}x_{cn}y_{cn}^2 \\
&- \frac{5\pi\rho_{cn}t_{cn}}{4l_n^2}x_{cn}^4 - \frac{3\pi\rho_{cn}t_{cn}}{2l_n^2}x_{cn}^2 y_{cn}^2 - \frac{\pi\rho_{cn}t_{cn}y_{cn}^4}{4l_n^2} - \frac{\pi\rho_{cn}t_{cn}y_{cn}}{K_{yn}l_n}x_{cn}^3 - \frac{\pi\rho_{cn}t_{cn}x_{cn}}{K_{yn}l_n}y_{cn}^3
\end{aligned}
\tag{A9}
$$

$$\begin{aligned} g_n =& \frac{I_{xbn}K_{xn}}{K_{yn}^2 l_n} - \frac{I_{xbn}}{K_{yn}^2} - \frac{I_{xybn}}{K_{yn}l_n} + \frac{\pi K_{xn}\rho_{cn}t_{cn}x_{cn}^4}{4K_{yn}^2 l_n} + \frac{3\pi K_{xn}\rho_{cn}t_{cn}x_{cn}^2}{2K_{yn}^2 l_n}y_{cn}^2 \\ &+ \frac{5\pi K_{xn}\rho_{cn}t_{cn}y_{cn}^4}{4K_{yn}^2 l_n} + \frac{m_{bn}y_{bn}}{K_{yn}} + \frac{\pi\rho_{cn}}{K_{yn}}t_{cn}x_{cn}^2 y_{cn} + \frac{\pi\rho_{cn}}{K_{yn}}t_{cn}y_{cn}^3 - \frac{\pi\rho_{cn}t_{cn}y_{cn}}{K_{yn}l_n}x_{cn}^3 \\ &- \frac{\pi\rho_{cn}t_{cn}x_{cn}}{K_{yn}l_n}y_{cn}^3 - \frac{\pi\rho_{cn}t_{cn}x_{cn}^4}{4K_{yn}^2} - \frac{3\pi\rho_{cn}t_{cn}}{2K_{yn}^2}x_{cn}^2 y_{cn}^2 - \frac{5\pi\rho_{cn}t_{cn}}{4K_{yn}^2}y_{cn}^4 \end{aligned} \tag{A10}$$

$$\begin{aligned} h_n =& \frac{I_{xbn}K_{xn}^2}{K_{yn}^2 l_n^2} - \frac{2I_{xybn}K_{xn}}{K_{yn}l_n^2} + \frac{I_{ybn}}{l_n^2} + \frac{\pi K_{xn}^2\rho_{cn}t_{cn}x_{cn}^4}{4K_{yn}^2 l_n^2} + \frac{3\pi K_{xn}^2\rho_{cn}t_{cn}x_{cn}^2}{2K_{yn}^2 l_n^2}y_{cn}^2 \\ &+ \frac{5\pi K_{xn}^2\rho_{cn}t_{cn}y_{cn}^4}{4K_{yn}^2 l_n^2} - \frac{2\pi K_{xn}\rho_{cn}}{K_{yn}l_n^2}t_{cn}x_{cn}^3 y_{cn} - \frac{2\pi K_{xn}\rho_{cn}}{K_{yn}l_n^2}t_{cn}x_{cn}y_{cn}^3 + \frac{5\pi\rho_{cn}t_{cn}}{4l_n^2}x_{cn}^4 \\ &+ \frac{3\pi\rho_{cn}t_{cn}}{2l_n^2}x_{cn}^2 y_{cn}^2 + \frac{\pi\rho_{cn}t_{cn}y_{cn}^4}{4l_n^2} \end{aligned} \tag{A11}$$

$$\begin{aligned} i_n =& -\frac{I_{xbn}K_{xn}}{K_{yn}^2 l_n} + \frac{I_{xybn}}{K_{yn}l_n} - \frac{\pi K_{xn}\rho_{cn}t_{cn}x_{cn}^4}{4K_{yn}^2 l_n} - \frac{3\pi K_{xn}\rho_{cn}t_{cn}x_{cn}^2}{2K_{yn}^2 l_n}y_{cn}^2 - \frac{5\pi K_{xn}\rho_{cn}t_{cn}y_{cn}^4}{4K_{yn}^2 l_n} \\ &+ \frac{\pi\rho_{cn}t_{cn}y_{cn}}{K_{yn}l_n}x_{cn}^3 + \frac{\pi\rho_{cn}t_{cn}x_{cn}}{K_{yn}l_n}y_{cn}^3 \end{aligned} \tag{A12}$$

$$j_n = \frac{I_{xbn}}{K_{yn}^2} + \frac{\pi\rho_{cn}t_{cn}x_{cn}^4}{4K_{yn}^2} + \frac{3\pi\rho_{cn}t_{cn}}{2K_{yn}^2}x_{cn}^2 y_{cn}^2 + \frac{5\pi\rho_{cn}t_{cn}}{4K_{yn}^2}y_{cn}^4 \tag{A13}$$

Appendix A.2. Mass Matrix for Linkages 2, 4, and 5

Linkages 2, 4, and 5 are defined by two basic points. For linkage 2, point A is considered as i while point C is considered as j; for linkage 4, point D is considered as i while point G is considered as j; for linkage 5, point F is considered as i while point G is considered as j. Each of them have their origin at point i and the x axis directed toward point j. For each linkage, l_n is the distance between points i and j.

By substituting the corresponding terms in the mass matrix of the elements defined by two basic points M_{2P} (equation can be found in [38]), it is possible to obtain the terms of the mass matrix of each of these elements consisting of a counterweight and a linkage (Equations (A14)–(A17)).

$$\begin{aligned} a_n =& m_{bn} + \pi\rho_{cn}t_{cn}\left(x_{cn}^2 + y_{cn}^2\right) - \frac{1}{l_n(m_{bn} + \pi\rho_{cn}t_{cn}(x_{cn}^2 + y_{cn}^2))} \\ &\left(2.0m_{bn} + 2.0\pi\rho_{cn}t_{cn}\left(x_{cn}^2 + y_{cn}^2\right)\right)\left(m_{bn}x_{bn} + \pi\rho_{cn}t_{cn}x_{cn}\left(x_{cn}^2 + y_{cn}^2\right)\right) \\ &+ \frac{1}{l_n^2}\left(I_{bn} + \pi\rho_{cn}t_{cn}x_{cn}^2\left(x_{cn}^2 + y_{cn}^2\right) + \pi\rho_{cn}t_{cn}y_{cn}^2\left(x_{cn}^2 + y_{cn}^2\right) + 0.5\pi\rho_{cn}t_{cn}\left(x_{cn}^2 + y_{cn}^2\right)^2\right) \end{aligned} \tag{A14}$$

$$\begin{aligned} b_n =& \frac{1}{l_n}\left(m_{bn}x_{bn} + \pi\rho_{cn}t_{cn}x_{cn}\left(x_{cn}^2 + y_{cn}^2\right)\right) \\ &- \frac{1}{l_n^2}\left(I_{bn} + \pi\rho_{cn}t_{cn}x_{cn}^2\left(x_{cn}^2 + y_{cn}^2\right) + \pi\rho_{cn}t_{cn}y_{cn}^2\left(x_{cn}^2 + y_{cn}^2\right) + 0.5\pi\rho_{cn}t_{cn}\left(x_{cn}^2 + y_{cn}^2\right)^2\right) \end{aligned} \tag{A15}$$

$$\begin{aligned} c_n =& \frac{1}{l_n(m_{bn} + \pi\rho_{cn}t_{cn}(x_{cn}^2 + y_{cn}^2))}\left(-m_{bn} - \pi\rho_{cn}t_{cn}\left(x_{cn}^2 + y_{cn}^2\right)\right) \\ &\left(m_{bn}y_{bn} + \pi\rho_{cn}t_{cn}y_{cn}\left(x_{cn}^2 + y_{cn}^2\right)\right) \end{aligned} \tag{A16}$$

$$d_n = \frac{1}{l_n^2}\left(I_{bn} + \pi\rho_{cn}t_{cn}x_{cn}^2\left(x_{cn}^2 + y_{cn}^2\right) + \pi\rho_{cn}t_{cn}y_{cn}^2\left(x_{cn}^2 + y_{cn}^2\right) + 0.5\pi\rho_{cn}t_{cn}\left(x_{cn}^2 + y_{cn}^2\right)^2\right) \quad \text{(A17)}$$

References

1. Arakelian, V.; Briot, S. *Balancing of Linkages and Robot Manipulators. Mechanisms and Machine Science*; Springer International Publishing: Cham, Switzerland, 2015; Volume 27.
2. Uicker, J.J.; Pennock, G.R.; Shigley, J.E. *Theory of Machines and Mechanisms*, 5th ed.; Oxford University Press: New York, NY, USA, 2016.
3. Waldron, K.J.; Kinzel, G.L. *Kinematics, Dynamics, and Design of Machinery*, 2nd ed.; John Wiley: Hoboken, NJ, USA, 2004.
4. Arakelian, V.; Dahan, M.; Smith, M.A. Historical review of the evolution of the theory on balancing of mechanisms. In *Symposium on History of Machines and Mechanisms Proceedings HMM 2000*; Ceccarelli, M., Ed.; Springer: Dordrecht, The Netherlands, 2000; pp. 291–300.
5. Arakelian, V. Inertia forces and moments balancing in robot manipulators: A review. *Adv. Robot.* **2017**, *31*, 717—726. [CrossRef]
6. Wei, B.; Zhang, D. A review of dynamic balancing for robotic mechanisms. *Robotica* **2021**, *39*, 55–71. [CrossRef]
7. Fisher, O. Über die reduzierten Systeme und die Hauptpunkte der Glieder eines Gelenkmechanismus und ihre Bedeutung für die technische Mechanik. *Z. Für Angew. Math. Und Phys.* **1902**, *47*, 429–466.
8. Goryachkin, V.P. The forces of inertia and their balancing. In *Collection of Scientific Works*; Kolos: Moscow, Russia, 1914; pp. 283–418.
9. Yudin, V. *The Balancing of Machines and Their Stability*; Edition of Academy of Red Army: Moscow, Russia, 1941; 124p.
10. Kreutzinger, R. Über die bewegung des Schwerpunktes beim Kurbelgetriebe. *Getriebetechnik* **1942**, *10*, 397–398.
11. Maxwell, R.L. *Kinematics and Dynamics of Machinery*, 1st ed.; Prentice Hall: Englewood Cliff, NJ, USA, 1960.
12. Smith, M.R.; Maundert, L. Inertia forces in a four-bar linkage. *J. Mech. Eng. Sci.* **1967**, *9*, 218–225. [CrossRef]
13. Talbourdet, G.L.; Shepler, P.R. Mathematical solution of 4-bar linkages-IV. Balancing of linkages. *Mach. Des.* **1941**, *13*, 73–77.
14. Lanchester, F.W. Engine Balancing. *Inst. Automob. Eng.* **1914**, *8*, 195–271. [CrossRef]
15. Root, R.E. *Dynamics of Engine and Shaft*; John Wiley: New York, NY, USA, 1932.
16. Artobolevsky, I.I.; Edelshtein, B.V. *Methods of Inertia Calculation for Mechanisms of Agricultural Machines*; Selkhozizdate: Moscow, Russia, 1935.
17. Gheronimus, Y.L. An approximate method of calculating a counterweight for the balancing of vertical inertia forces. *Mechanisms* **1968**, *3*, 283–288. [CrossRef]
18. Doucet, E. Équilibrage dynamique des moteurs en ligne. *Tech. Automob. Arienne* **1946**, *37*, 30–31.
19. Emod, I.; Jurek, A. Massenausgleich am Kurbelgetriebe von Sechszylinder-viertakt-V-motoren mit 6 Kurbeln und 60 Zylinder-winkeln. *Period. Polytech. Mech. Eng.* **1967**, *3–4*, 205–211.
20. Semenov, M.V. The synthesis of partly balanced plane mechanisms. *Mechanisms* **1968**, *3*, 339–353. [CrossRef]
21. Berkof R.S.; Lowen, G.G. A new method for complete force balancing simple linkages. *J. Eng. Ind.* **1969**, *91B*, 21–26. [CrossRef]
22. Smith, M.R. Dynamic analysis and balancing of linkages with interactive computer graphics. *Comput. Aided Des.* **1975**, *7*, 15–19. [CrossRef]
23. Tepper, F.R.; Lowen, G.G. General theorems concerning full force balancing of planar linkages by internal mass redistribution. *J. Eng. Ind.* **1972**, *94*, 789–796. [CrossRef]
24. Berkof, R.S. Complete force and moment balancing of inline four-bar linkages. *Mech. Mach. Theory* **1973**, *8*, 397–410. [CrossRef]
25. Wiederrich, J.L.; Roth, B. Momentum balancing of four-bar linkages. *J. Manuf. Sci. Eng.* **1976**, *4*, 1289–1295. [CrossRef]
26. Dresig, H.; Jacobi, P. Vollständiger trägheitskraftausgleich von ebenen koppelgetrieben durch anbringen eines zweischlages. *Maschinenbautechnik* **1974**, *23*, 5–8.
27. Feng, G. Complete Shaking Force and Shaking Moment balancing of four types of six-bar linkages. *Mech. Mach. Theory* **1989**, *24*, 275–287. [CrossRef]
28. Kochev, I.S. Active balancing of the frame Shaking Moment in high speed planar machines. *Mech. Mach. Theory* **1992**, *27*, 53–58. [CrossRef]
29. de Jong, J.J.; van Dijk, J.; Herder, J.L. A screw based methodology for instantaneous dynamic balance. *Mech. Mach. Theory* **2019**, *141*, 267–282. [CrossRef]
30. Acevedo, M.; Orvañanos-Guerrero, M.T.; Velázquez, R.; Arakelian, V. An alternative method for Shaking Force balancing of the 3RRR PPM through acceleration control of the center of mass. *Appl. Sci.* **2020**, *10*, 1351. [CrossRef]
31. Meijaard, J.P.; van der Wijk, V. Dynamic balancing of mechanisms with flexible links. *Mech. Mach. Theory* **2022**, *172*, 104784. [CrossRef]
32. Segla, S.; Kalker-Kalman, C.M.; Schwab, A.L. Statical balancing of a robot mechanism with the aid of a genetic algorithm. *Mech. Mach. Theory* **1998**, *33*, 163–174. [CrossRef]
33. Farmani, M.; Jaamialahmadi, A.; Babaie, M. Multiobjective optimization for force and moment balance of a four-bar linkage using evolutionary algorithms. *J. Mech. Sci. Technol.* **2011**, *25*, 2971–2977. [CrossRef]
34. Zamuda, A.; Brest, J.; Boskovic, B.; Zumer V. Differential evolution for multiobjective optimization with self adaptation. In Proceedings of the 2007 IEEE Congress on Evolutionary Computation, Singapore, 25–28 September 2007.

35. Erkaya, S. Investigation of balancing problem for a planar mechanism using genetic algorithm. *J. Mech. Sci. Technol.* **2013**, *27*, 2153–2160. [CrossRef]
36. Bošković, M.; Šalinić, S.; Bulatović, R.; Miodragović, G. Multiobjective optimization for dynamic balancing of four-bar mechanism. In Proceedings of the 6th International Congress of Serbian Society of Mechanics, Mountain Tara, Serbia, 19–21 June 2017.
37. García de Jalón, J. Twenty-five years of natural coordinates. *Multibody Syst. Dyn.* **2007**, *18*, 15–33. [CrossRef]
38. Orvañanos-Guerrero, M.T.; Sánchez, C.N.; Rivera, M.; Acevedo, M.; Velázquez, R. Gradient descent-based optimization method of a four-bar mechanism using Fully Cartesian coordinates. *Appl. Sci.* **2019**, *9*, 4115. [CrossRef]
39. Acevedo, M.; Orvañanos-Guerrero, M.T.; Velázquez, R.; Haro, E. Optimum balancing of the four-bar linkage using Fully Cartesian coordinates. *IEEE Lat. Am. Trans.* **2019**, *17*, 983–990. [CrossRef]
40. Bourbonnais, F.; Bigras, P.; Bonev, I.A. Minimum-time trajectory planning and control of a pick-and-place five-bar parallel robot. *IEEE/ASME Trans. Mechatron.* **2015**, *20*, 740–749. [CrossRef]
41. Wang, D.; Wang, L.; Wu, J.; Ye, H. An experimental study on the dynamics calibration of a 3-DOF parallel tool head *IEEE/ASME Trans. Mechatron.* **2019**, *24*, 2931–2941.
42. Pennock, G.R.; Israr, A. Kinematic analysis and synthesis of an adjustable six-bar linkage *Mech. Mach. Theory* **2009**, *44*, 306–323. [CrossRef]
43. García de Jalón, J.; Bayo, E. *Kinematic and Dynamic Simulation of Multibody Systems: The Real-Time Challenge*; Springer: New York, NY, USA, 1994.
44. Storn, R.; Price, K. Differential evolution-a simple and efficient heuristic for global optimization over continuous spaces. *J. Glob. Optim.* **1997**, *11*, 341–359. [CrossRef]
45. Das, A.K.; Mishra, D.; Das, K.; Mallick, P.K.; Kumar, S.; Zymbler, M.; El-Sayed, H. Prophesying the short-term dynamics of the crude oil future price by adopting the survival of the fittest principle of improved grey optimization and extreme learning machine. *Mathematics* **2022**, *10*, 1121. [CrossRef]
46. Álvarez Gutiérrez, D.; Sánchez Lasheras, F.; Martín Sánchez, V.; Suárez Gómez, S.L.; Moreno, V.; Moratalla-Navarro, F.; Molina de la Torre, A.J. A new algorithm for multivariate genome wide association studies based on differential evolution and extreme learning machines. *Mathematics* **2022**, *10*, 1024. [CrossRef]
47. Bergstra, J.; Bengio, Y. Random search for hyper-parameter optimization. *J. Mach. Learn. Res.* **2012**, *13*, 281–305.
48. Etesami, G.; Felezi, M.E.; Nariman-Zadeh, N. Pareto optimal multi-objective dynamical balancing of a slider-crank mechanism using differential evolution algorithm. *Int. J. Automot. Eng.* **2019**, *9*, 3021–3032.
49. Chaudhary, K.; Chaudhary, H. Optimal design of planar slider-crank mechanism using teaching-learning-based optimization algorithm. *J. Mech. Sci. Technol.* **2015**, *29*, 5189–5198. [CrossRef]
50. Chaudhary, K.; Chaudhary, H. Optimum balancing of slider-crank mechanism using equimomental system of point-masses. *Procedia Technol.* **2014**, *14*, 35–42. [CrossRef]
51. Orvañanos-Guerrero, M.T.; Acevedo, M.; Sánchez, C.N.; Giannoccaro, N.I.; Visconti, P.; Velázquez, R. Efficient balancing optimization of a simplified slider-crank mechanism. In Proceedings of the 2020 IEEE ANDESCON, Quito, Ecuador, 13–16 October 2020.
52. Chaudhary, K.; Chaudhary, H. Shape optimization of dynamically balanced planar four-bar mechanism. *Procedia Comput. Sci.* **2015**, *57*, 519–526. [CrossRef]
53. Belleri B.K.; Kerur, S.B. Balancing of planar six-bar mechanism with genetic algorithm. *J. Mech. Energy Eng.* **2020**, *4*, 303–308. [CrossRef]
54. Hernández, E.; Velázquez, R.; Macías-Quijas, R.; Pissaloux, E.; Giannoccaro, N.I.; Lay-Ekuakille, A. Kinematic computations for small-size humanoid robot KUBO. *ARPN J. Eng. Appl. Sci.* **2017**, *12*, 7311–7320.
55. Xu, K.; Liu, H.; Zhu, X.; Song, Y. Kinematic analysis of a novel planar six-bar bionic leg. *Mech. Mach. Sci.* **2019**, *73*, 13–21.
56. Velázquez, R.; Garzón-Castro, C.L.; Acevedo, M.; Orvañanos-Guerrero, M.T.; Ghavifekr, A.A. Design and characterization of a miniature bio-inspired mobile robot. In Proceedings of the 2021 12th International Symposium on Advanced Topics in Electrical Engineering, Bucharest, Romania, 25–27 March 2021.
57. Shao, Y.; Xiang, Z.; Liu, H.; Li, L. Conceptual design and dimensional synthesis of cam-linkage mechanisms for gait rehabilitation. *Mech. Mach. Theory* **2016**, *104*, 31–42. [CrossRef]